Manipulating one- and two-dimensional stimulated-x-ray resonant-Raman signals in molecules by pulse polarizations

Daniel Healion, Jason D. Biggs, and Shaul Mukamel*
Department of Chemistry, University of California Irvine, Irvine, California 92697, USA
(Received 18 February 2012; published 28 September 2012)

The simulation of spontaneous (RIXS) and stimulated x-ray Raman scattering (SXRS) signals in isotropic samples requires rotational averaging of a fourth-rank tensor product of two polarizabilities. Attosecond stimulated x-ray Raman spectroscopy excites multiple valence transitions covered by the pulse bandwidths. These excitations depend on the orientation of the molecule with respect to the pulse polarizations in the laboratory frame, making the response a high-rank tensor operator. Many contributions to the response coming from different tensor components complicate the analysis and interpretation of these measurements. By using the magic angle between the excitation and detection fields these signals may be expressed as correlation functions of the scalar isotropic polarizabilities, which greatly simplifies their interpretation. We show that a similar simplification of three-pulse two-dimensional stimulated x-ray Raman scattering (2D-SXRS), which depends on a rotationally averaged sixth-rank tensor, is possible by a super magic angle (SMA) combination of two measurements with specific pulse polarization configurations. Calculated SMA 2D-SXRS signals for *trans-N*-methylacetamide (NMA) at the nitrogen *K* edge reveal different features compared with the all-parallel polarization configuration.

DOI: 10.1103/PhysRevA.86.033429 PACS number(s): 33.20.Rm, 42.65.Re, 42.55.Vc, 82.53.Hn

I. INTRODUCTION

New x-ray laser sources will soon enable nonlinear time-domain spectroscopy in the x-ray regime [1–4]. Parametric down conversion [5] and pump-probe spectra [6] have already been reported. Traditionally, nonlinear techniques have employed a large number of experimental controls for measuring the material response, including the wave vectors, pulse polarizations, phases, frequencies, time delays, and even the quantum characteristics of the applied fields [7–10]. The increase in the number of controllable parameters and the richness of their interplay may come at the expense of a simple interpretation of the underlying dynamics; designing an experiment which reveals interesting characteristics of the system is not obvious. We focus in this article on the effect of the applied pulse polarizations to two-dimensional stimulated x-ray Raman spectroscopy (2D-SXRS) [11], an extension of one-dimensional SXRS (1D-SXRS) where the sample is subjected to three broadband pulses and the signal is the integrated transmitted intensity of the third pulse relative to the signal without the other two pulses. Vibrational stimulated Raman spectroscopy makes use of the Franck-Condon approximation, in which the transition dipole coupling the system to the field is only weakly dependent on the nuclear coordinates. The applied perturbation which launches and measures the nuclear wave packet is a scalar operator in this approximation.

The perturbation in attosecond stimulated x-ray Raman spectroscopy, in which a pulse bandwidth can excite multiple valence transitions, is a tensor operator. The many contributions to the response from different tensor components may obscure the dynamics of the valence electronic wave packet. To resolve this problem, we propose a super magic angle (SMA) pulse polarization configuration where the signal is given exclusively in terms of the scalar isotropic part of the polarizability tensor. This technique is a higher-order analog of the magic angle between pump and probe pulse polarizations in 1D stimulated Raman experiments.

Impulsive stimulated Raman spectroscopies measure the change in absorbance of a probe pulse after excitation with one (1D-SRS) or a pair of pulses (2D-SRS). Intensity requirements for observing stimulated x-ray Raman signals were given in Refs. [11,12]. Time-domain x-ray resonance Raman spectroscopy (see Fig. 1) uses a fast, high-frequency, core-excited state as an intermediate in a Raman process to prepare and probe a wave packet of slow, low-frequency, valence excited states [9,13]. The 1D-SXRS technique resonant with core-transitions was proposed and simulated for tight-binding models of linear organic chains and small molecules [14–16] and represents an extension of IR and optical-pump–x-ray-probe techniques [6,17,18]. Experimental techniques to develop pulses that can perform these experiments are being pursued [19]. 1D-SRS signals with impulsive pulses can be written as correlation functions of the dynamic polarizability α_j averaged over the envelope of pulse j that can be shaped to selectively excite resonances within its bandwidth. The polarizability α is a second rank tensor with Cartesian components $\alpha_{xx},\alpha_{xy},\ldots$, etc. The specific linear combinations of their products which form the signal are controlled by the pulse polarizations [20].

This tensor operator can also be represented in a polar basis [21]. For all-parallel polarized pulses every possible pairwise contraction of these tensor elements contributes to the signal [22]. The spectral bandwidth of x-ray pulses may cover intermediate states with different orientations of transition dipole moments. Stimulated resonance Raman experiments with optical pulses usually select one intermediate electronic state. In this case all the material transition dipoles are parallel,

*smukamel@uci.edu

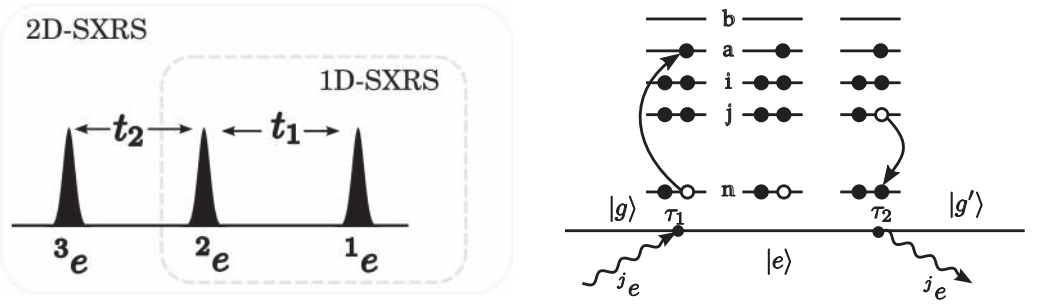

FIG. 1. (Left) Pulse sequence for 1D (two pulse) and 2D (three pulse) SXRS experiments. (Right) The x-ray stimulated Raman process.

and the signal is independent of the polarization. Stimulated x-ray techniques contain a large number of core-excited states with distinguishable transition dipoles in the bandwidth of each pulse. We thus expect strong polarization effects of the signal. The magic polarization angle between pulse polarizations in the two-pulse 1D spectroscopy disentangles the various tensor components, and the response is simply given by a correlation function of the scalar isotropic polarizability $\bar{\alpha} = (\alpha_{xx} + \alpha_{yy} + \alpha_{zz})/3$. The signal can be viewed in terms of the evolution of a wave packet created by this scalar operator. Here we show that a similar simplification of the signal can be achieved in three-pulse 2D-SRS by a supermagic angle (SMA) combination of two separate experiments with different pulse polarization configurations.

Polarization-dependent off-resonant Raman spectroscopy with optical pulses has been applied to study intermolecular vibrations in liquids. Coherent control and pulse polarization techniques have been used to resolve higher-order processes relative to lower-order processes, or cascades, in off-resonant stimulated Raman experiments [23–25]. Various polarization and phase-matching directions that amplify the higher-order terms compared to the cascades were identified. Heterodyne detection was applied towards the same goal [26] using the "Dutch Cross" polarization combination [27]. Polarization-dependent four-wave mixing techniques may be used to study molecular chirality in vibrational and electronic transitions [28] The polarization dependence of the fifth-order Raman signal in strongly coupled vibrational systems was addressed in a series of earlier papers [29,30].

The 2D-SXRS signal was recently calculated [11]. We address the decomposition of the tensor response function into isotropic and anisotropic parts in an ensemble of randomly oriented molecules, and show that the sum of two signals taken with noncollinear pulses can be used to extract the isotropic part of the 2D-SXRS signal. We further compare the SMA and all-parallel signals for the 1D-SXRS and 2D-SXRS stimulated x-ray Raman spectra of the nitrogen K edge of *trans*-NMA. The Raman process is illustrated in Fig. 1. Interaction with the first pulse excites a core electron into an unoccupied orbital, preparing a wave packet of valence electronic states, and the second induces a stimulated emission of an occupied orbital into the core, leaving a particle-hole excitation. In 1D-SXRS the projection of these single particle-hole excitations onto the valence excited states $|g'\rangle$ results in a superposition which evolves during the time delay t_1, until it is probed by a second pulse. The dimensionality of the technique is given by the number of experimentally controlled delay periods between pulses.

We first describe the one-dimensional Raman process, which will set the stage for extending the same formalism to 2D-SXRS. We note an interesting fact about the polarization dependence of the 1D signal. It is usually assumed that the time-dependent 1D stimulated Raman signal is the Fourier transform of the frequency domain spontaneous Raman (RIXS) [31–33]. Both may be expressed as time- or frequency-dependent products of the molecular polarizabilities. For pulses whose bandwidth spans several electronic transitions these polarizabilities are tensor operators. For spontaneous Raman (Fig. 2), the polarization of the applied ($\hat{e}_L$, green) and detected ($\hat{e}_S$, red) light can be varied independently. In the stimulated Raman process (Fig. 3), the relative polarizations of the first ($\hat{e}_1$, red) and the second ($\hat{e}_2$, green) pulse are under experimental control. This difference allows the isotropic part of the 1D response, which is irretrievably mingled with other contributions in the frequency domain, to be recovered in the time-dependent "magic angle" signal, in which the polarizabilities contributing to the response can be represented as scalars instead of dyadic tensors. The same approach is then extended to the polarization-dependent 2D-SXRS signal. We show that even though it is not possible to have a single 2D-SXRS pulse polarization configuration where the signal depends solely on the isotropic polarizability, the average of two, separately measured 2D-SXRS signals with different pulse polarizations can achieve that goal. Simulations of the all-parallel and SMA 2D-SXRS signals for *trans*-NMA are presented.

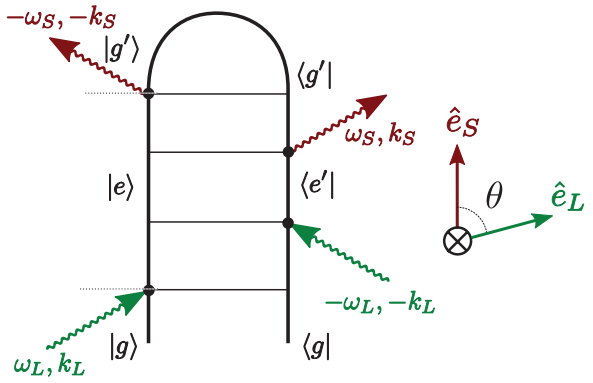

FIG. 2. (Color online) Loop diagram for RIXS.

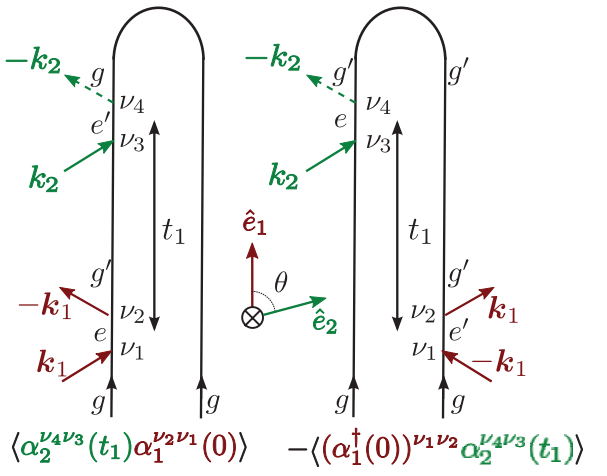

FIG. 3. (Color online) 1D-SXRS diagrams.

II. ROTATIONALLY AVERAGED 1D RAMAN SIGNALS

A. Polarization variation of RIXS

Tensor expressions for nonlinear optical signals were derived in [20] and applied to calculate photon echo signals for vibrational and electronic excitonic systems [28]. The theory of polarization-dependent RIXS in homonuclear core-excited systems was described in [34], and the anisotropic contributions to the RIXS response were studied in [35]. We summarize these results below for comparison with the 1D-SXRS signal. The frequency domain RIXS signal is represented as a single diagram in the Keldysh-loop formalism [36], shown in Fig. 2. We define the molecular transition polarizability in the rotating wave approximation as

$$\tilde{\alpha}_{g'g}^{\nu_2\nu_1}(\omega_L) = \sum_e \frac{\mu_{g'e}^{\nu_2}\mu_{eg}^{\nu_1}}{\omega_L - \epsilon_e + i\gamma_e}. \tag{1}$$

The superscripts $\nu_1,\nu_2,\ldots$ are Cartesian tensor indices in the molecular frame, and $f_1,f_2,\ldots$ are indices in the laboratory (field) frame. Subscripts $g,g',e,\ldots$ denote matrix elements of the quantum operators α and μ between ground ($|g\rangle$), valence excited ($|g',g''\rangle$), and core excited ($|e,e'\rangle$) states. We use atomic units for all eigenstate energies, lifetimes, pulse frequencies, and widths. The RIXS signal, shown in Fig. 2, is described by the Kramers-Heisenberg expression,

$$S_{\rm RIXS}(\omega_L,\omega_S) = \sum_{g'}\sum_{\nu_1\nu_2\nu_3\nu_3} \tilde{\alpha}_{g'g}^{\nu_2\nu_1}(\omega_L)\tilde{\alpha}_{gg'}^{\nu_3\nu_4*}(\omega_L) \times \delta_{\gamma_{g'}}(\omega_L - \omega_S - \epsilon_{g'}). \tag{2}$$

A Lorentzian with a linewidth given by the valence excited state lifetimes $\gamma_{g'}$,

$$\delta_\gamma(\omega - \epsilon_{g'}) = \frac{1}{\pi}\frac{2\pi\gamma}{(\omega-\epsilon_{g'})^2+\gamma^2}, \tag{3}$$

is used in the simulations. The rotationally averaged RIXS signal in an isotropic ensemble contains three contributions [34]:

$$S_{\rm RIXS}(\omega_L,\omega_S) = \tfrac{1}{30}(3\cos^2\theta - 1)S_A(\omega_L,\omega_S) + \tfrac{1}{30}(3\cos^2\theta - 1)S_B(\omega_L,\omega_S) + \tfrac{1}{30}(4 - 2\cos^2\theta)S_C(\omega_L,\omega_S). \tag{4}$$

θ is the angle between the applied field polarization $\hat{e}_L$ and the polarization of the scattered mode $\hat{e}_S$. These contributions depend on different contractions of the polarizability. The isotropic part of the signal is

$$S_A(\omega_L,\omega_S) = \sum_{g'}\sum_{\nu_1\nu_2}\tilde{\alpha}_{g'g}^{\nu_1\nu_1}(\omega_L)\tilde{\alpha}_{gg'}^{\nu_2\nu_2*}(\omega_L)\delta_{\gamma_{g'}}(\omega_L-\omega_S-\epsilon_{g'}) = \sum_{g'}\bar{\alpha}_{1;g'g}(\omega_L)\bar{\alpha}^*_{1;gg'}(\omega_L)\delta_{\gamma_{g'}}(\omega_L-\omega_S-\epsilon_{g'}), \tag{5}$$

where the isotropic scalar polarizability for the electronic states r,s

$$\bar{\alpha}_{rs} = \tfrac{1}{3}{\rm Tr}[\alpha_{rs}] = (1/3)\left(\alpha_{rs}^{xx}+\alpha_{rs}^{yy}+\alpha_{rs}^{zz}\right), \tag{6}$$

is defined as the trace over the diagonal parts of the tensor α. The anisotropic parts are

$$S_B(\omega_L,\omega_S) = \sum_{g'}\sum_{\nu_1\nu_2}\tilde{\alpha}_{g'g}^{\nu_2\nu_1}(\omega_L)\tilde{\alpha}_{gg'}^{\nu_2\nu_1*}(\omega_L)\delta_{\gamma_{g'}}(\omega_L-\omega_S-\epsilon_{g'}), \tag{7}$$

and

$$S_C(\omega_L,\omega_S) = \sum_{g'}\sum_{\nu_1\nu_2}\tilde{\alpha}_{g'g}^{\nu_2\nu_1}(\omega_L)\tilde{\alpha}_{gg'}^{\nu_1\nu_2*}(\omega_L)\delta_{\gamma_{g'}}(\omega_L-\omega_S-\epsilon_{g'}). \tag{8}$$

The RIXS experiment with a magic angle (MA) between the incident and scattered polarizations, where $3\cos^2\theta - 1 = 0$ ($\theta_{\rm MA} = 54.7^\circ$), can isolate the $S_C(\omega_L,\omega_S)$ part of the anisotropic polarizability. The isotropic polarizability $S_A(\omega_L,\omega_S)$ is irretrievably mixed with the anisotropic part $S_B(\omega_L,\omega_S)$. It is thus not possible to extract the purely isotropic signal $S_A(\omega_L,\omega_S)$ from RIXS measurements. Below we show that, thanks to a different form of polarization control, the time-domain 1D-SXRS technique can do that.

B. Polarization-dependent 1D-SXRS

The electric field in a 1D-SXRS experiment consists of two pulses:

$$E(t) = \mathscr{E}_2(t-t_1)e^{-i\omega_2(t-t_1)} + \mathscr{E}_1(t)e^{-i\omega_1 t} + {\rm c.c.}, \tag{9}$$

separated by a delay t_1. We assume Gaussian envelopes,

$$\mathscr{E}_j(t) = \frac{1}{\sigma_j\sqrt{2\pi}}\exp[t^2/2\sigma_j^2]\,\hat{e}_j; \quad j = 1,2, \tag{10}$$

with temporal full width at half maximum $2\sqrt{2\ln 2}\sigma_j$, central frequencies ω_j, and unit polarization vectors $\hat{e}_j$. The two diagrams shown in Fig. 3 yield two contributions to the signal,

$$S^{1D}(t_2,t_1) = {\rm Re}[\langle\alpha_2(t_1)\alpha_1(0)\rangle - \langle\alpha_1^\dagger(0)\alpha_2(t_1)\rangle]. \tag{11}$$

1D-SXRS depends on the two effective polarizability operators α_1 and α_2 which account for broadband excitation

with each pulse,

$$\alpha^{\nu_2\nu_1}_{j;g'g''} = \sum_e \frac{\mu^{\nu_2}_{g'e}\mu^{\nu_1}_{eg''}}{2\pi}\int_{-\infty}^{\infty}\frac{\varepsilon^*_j(\omega)\varepsilon_j(\omega-\omega_{g''g'})}{\omega-\omega_{eg''}+\omega_j+i\gamma_e}d\omega. \quad (12)$$

This definition of the polarizability differs from the RIXS polarizability in Eq. (1) as the same mode of the field (j) interacts twice with the system during the Raman process. In RIXS, a photon is absorbed from one mode of the field and scattered into another. These effective polarizability operators are second-order tensor objects and operators in the space of valence electronic excitations $\{g,g',\dots\}$ [13]. The time-dependent polarizability operators are (see Fig. 3)

$$\alpha^{\nu_2\nu_1}_j(t) = \sum_{rs}\alpha^{\nu_2\nu_1}_{j;rs}\exp(i\omega_{rs}t-\Gamma_{rs}t)|r\rangle\langle s|. \quad (13)$$

Γ_{rs} is a dephasing of the $|r\rangle\langle s|$ coherence between valence excitations. The adjoint of this tensor operator is

$$(\alpha^\dagger_j)^{\nu_1\nu_2}_{sr}(-t) = \alpha^{\nu_2\nu_1*}_{j;rs}\exp(-i\omega_{rs}t-\Gamma_{rs}t). \quad (14)$$

The brackets in Eq. (11) $\langle\dots\rangle \equiv \mathrm{Tr}[\dots\rho_o]$ represent the trace over the equilibrium density matrix of valence electronic states. When the x-ray pulses are tuned off-resonant from any core excitations, $\alpha=\alpha^\dagger$, and the signal in Eq. (11) can be written as a response function, $S^{1D}_{\text{off-res}}(t_1)=\mathrm{Re}\langle[\alpha_2(t_1),\alpha_1(0)]\rangle$.

Starting from the time-domain 1D-SXRS signal given in Eq. (11), the full tensor form of the signal [11] is

$$S^{(1D)}_{\text{SXRS}}(\nu_1\nu_2\nu_3\nu_4;t_1) = \sum_{g'}\mathrm{Re}\Big[\big(\alpha^{\nu_4\nu_3}_{2;gg'}\big)\big(\alpha^{\nu_2\nu_1}_{1;g'g}\big)e^{-i\epsilon_{g'}t_1-\gamma_{g'}t_1} - \big(\alpha^{\nu_1\nu_2*}_{1;gg'}\big)\big(\alpha^{\nu_3\nu_4}_{2;g'g}\big)e^{+i\epsilon_{g'}t_1-\gamma_{g'}t_1}\Big]. \quad (15)$$

The rotationally averaged signal is given by contracting the tensor components in Eq. (15)

$$S^{(1D)}_{\text{SXRS}}(\tau,\theta) = \sum_{\nu_1\dots\nu_4 f_1\dots f_4} S^{(1D)}_{\text{SXRS}}(\nu_1\nu_2\nu_3\nu_4;\tau)I_{\nu_1\dots\nu_4;f_1\dots f_4}e^{f_1}_1e^{f_2}_1e^{f_3}_2e^{f_4}_2, \quad (16)$$

where $e^{f_j}_i$ is a tensor component f_j of the ith pulse, and the isotropic tensor is a geometric factor [20],

$$I_{\nu_1\dots\nu_4;f_1\dots f_4} = \mathbf{V}^T_L\mathbf{M}\mathbf{V}_R = \tfrac{1}{30}\begin{pmatrix}\delta_{\nu_1\nu_2}\delta_{\nu_3\nu_4}\\ \delta_{\nu_1\nu_3}\delta_{\nu_2\nu_4}\\ \delta_{\nu_1\nu_4}\delta_{\nu_2\nu_3}\end{pmatrix}^T\begin{pmatrix}4&-1&-1\\-1&4&-1\\-1&-1&4\end{pmatrix}\times\begin{pmatrix}\delta_{f_1f_2}\delta_{f_3f_4}\\ \delta_{f_1f_3}\delta_{f_2f_4}\\ \delta_{f_1f_4}\delta_{f_2f_3}\end{pmatrix}. \quad (17)$$

After contraction over the field tensor components, the signal $S^{(1D)}_{\text{SXRS}}(\tau,\theta)$ in Eq. (16) depends on θ, the angle between the pulse polarizations. The indices ν_i (f_i) represent tensor components of the transition dipole (pulse polarization) vectors. Each $\delta_{\nu_1\nu_2}$ arises from a tensor contraction over the indices ν_1 and ν_2. For the field polarization vectors each Kronecker delta in Eq. (17) represents a dot product after performing the contractions in Eq. (16):

$$\sum_{f_1f_2}e^{f_1}_1\delta_{f_1f_2}e^{f_2}_2 = (\hat{e}_1\cdot\hat{e}_2) = \cos\theta, \quad (18)$$

which is dependent on the angle between the polarizations of the applied pulses θ. Contractions of the second-rank tensors $\alpha^{\nu_1\nu_2}$ can be written as traces (in polarization space) over matrix products of these operators. After contraction, the signal in Eq. (16) is finally given by

$$S^{1D}_{\text{pol}}(\theta) = \tfrac{1}{30}\mathrm{Re}\begin{pmatrix}S_I(t_1)\\S_{II}(t_1)\\S_{III}(t_1)\end{pmatrix}\begin{pmatrix}4&-1&-1\\-1&4&-1\\-1&-1&4\end{pmatrix}\begin{pmatrix}1\\\cos^2\theta\\\cos^2\theta\end{pmatrix}. \quad (19)$$

Equation (19) is a weighted sum of three terms,

$$S^{(1D)}_{\text{SXRS}}(t_1) = \tfrac{1}{30}(4-\cos^2\theta)S_{\text{I}}(t_1) + \tfrac{1}{30}(3\cos^2\theta-1)\times[S_{II}(t_1)+S_{III}(t_1)], \quad (20)$$

mixed by a parametric dependence on θ:

$$S_I(t_1) = \sum_{g'}\sum_{\nu_1\nu_2}\mathrm{Re}\Big[\big(\alpha^{\nu_2\nu_2}_{2;gg'}\big)\big(\alpha^{\nu_1\nu_1}_{1;g'g}\big)e^{-i\epsilon_{g'}t_1-\gamma_{g'}t_1} - \big(\alpha^{\nu_1\nu_1*}_{1;gg'}\big)\big(\alpha^{\nu_2\nu_2}_{2;g'g}\big)e^{+i\epsilon_{g'}t_1-\gamma_{g'}t_1}\Big], \quad (21)$$

$$S_{II}(t_1) = \sum_{g'}\sum_{\nu_1\nu_2}\mathrm{Re}\Big[\big(\alpha^{\nu_2\nu_1}_{2;gg'}\big)\big(\alpha^{\nu_2\nu_1}_{1;g'g}\big)e^{-i\epsilon_{g'}t_1-\gamma_{g'}t_1} - \big(\alpha^{\nu_1\nu_2*}_{1;gg'}\big)\big(\alpha^{\nu_1\nu_2}_{2;g'g}\big)e^{+i\epsilon_{g'}t_1-\gamma_{g'}t_1}\Big], \quad (22)$$

and

$$S_{III}(t_1) = \sum_{g'}\sum_{\nu_1\nu_2}\mathrm{Re}\Big[\big(\alpha^{\nu_1\nu_2}_{2;gg'}\big)\big(\alpha^{\nu_2\nu_1}_{1;g'g}\big)e^{-i\epsilon_{g'}t_1-\gamma_{g'}t_1} - \big(\alpha^{\nu_1\nu_2*}_{1;gg'}\big)\big(\alpha^{\nu_2\nu_1}_{2;g'g}\big)e^{+i\epsilon_{g'}t_1-\gamma_{g'}t_1}\Big]. \quad (23)$$

The Fourier transform of these signals is given in Appendix D, and consists of a linear combination of Lorentzian peaks whose strength and relative mix of absorptive or dispersive lineshapes are controlled by the modulus and argument of the polarizabilities $\alpha_{g'g}$. The components S_I,S_{II}, and S_{III} differ only by their tensor contractions; each contains two terms represented by the diagrams in Fig. 3.

Selecting a particular pulse polarization configuration fixes the linear combination of tensor components of each α in Eq. (11) that contribute to the measured signal. By setting the angle between the pump and probe pulses to the magic angle (MA) we get

$$\bar{S}^{1D}_{\text{MA}}(t_1) = \mathrm{Re}[\langle\bar{\alpha}_2(t_1)\bar{\alpha}_1(0)\rangle - \langle\bar{\alpha}^\dagger_1(0)\bar{\alpha}_2(t_1)\rangle]. \quad (24)$$

The signal is now given by a correlation function of the scalar isotropic polarizability, rather than the second rank tensor operators in Eq. (11); this greatly simplifies the description and analysis of the response.

It follows from Eq. (24) that 1D-SXRS, unlike RIXS, can experimentally discriminate between the isotropic and anisotropic polarizabilities. This stems from the different polarization controls in the two experiments, as is clear by comparing the loop diagram for the RIXS process (Fig. 2) and the 1D-SXRS technique (Fig. 3). The selection in RIXS of the angle between the applied and measured scattered modes of the field leads to a different polarization dependence then in the 1D-SXRS, where only the polarization between pulses can be controlled.

C. Simulations

We now present simulations of the one- and two-dimensional stimulated and spontaneous x-ray Raman signals at the nitrogen K edge for the model system *trans-N*-methyl acetamide (*trans*-NMA). Details of the electronic structure calculations were given in earlier works [11,16]. The 1D signals presented here all use identical Gaussian pulses, defined in Eqs. (9) and (10). We set $\sigma_j = 77$ as (frequency FWHM in intensity $\simeq$14.2 eV) for all pulses, and set $\omega_j = 401.7$ eV resonant at the nitrogen K edge. For valence-excited states we use a lifetime broadening of $\gamma_{g'} = 0.05$ eV to visualize peak positions, and for core-excited states we take $\gamma_e = 0.085$ eV for the nitrogen and $\gamma_e = 0.10$ eV for the oxygen K-edge inverse lifetime as was used in prior studies [11,16].

For a fixed molecular orientation relative to the field the polarizabilities contributing to RIXS and 1D-SXRS can be expanded as a sum of transition dipole dot products:

$$\sum_{e,e'}(\vec{\mu}_{ge'}\cdot e_4)(\mu_{e'g'}\cdot e_3)(\mu_{g'e}\cdot e_2)(\mu_{eg}\cdot e_1) = \delta_{\nu_4 f_4}\delta_{\nu_3 f_3}\delta_{\nu_2 f_2}\delta_{\nu_1 f_1}. \quad (25)$$

For an isotropic distribution of molecules, $\delta_{\nu_4 f_4}\delta_{\nu_3 f_3}\delta_{\nu_2 f_2}\delta_{\nu_1 f_1}$ depends on the Euler rotation angles between the molecular and laboratory frames and Eq. (25) becomes

$$\int d\hat{l}\sum_{\nu_1\ldots\nu 4}\sum_{f_1\ldots f_4} l_{\nu_1 f_1} l_{\nu_2 f_2} l_{\nu_3 f_3} l_{\nu_4 f_4}. \quad (26)$$

An analytic form of the integral in Eq. (26) was presented in Ref. [20]. The result is a weighted sum of field vector and transition dipole dot products and the angles between the transition dipoles only (see Appendix E for details). For a given set of field polarizations, we get

$$\delta_{m_4 f_4}\delta_{m_3 f_3}\delta_{m_2 f_2}\delta_{m_1 f_1} = c_1\delta_{m_1 m_2}\delta_{m_3 m_4} + c_2\delta_{m_1 m_3}\delta_{m_2 m_4} + c_3\delta_{m_1 m_4}\delta_{m_2 m_3}. \quad (27)$$

c_1, c_2, and c_3 are responsible for S_A, S_B in RIXS and S_C, and S_I, S_{II}, and S_{III} for 1D-SXRS. The terms c_1 and c_2 depend on products of dot products between absorption and emission dipoles, while the c_3 term depends only on their squared magnitudes. By the Schwarz inequality, $(\vec{a}\cdot\vec{b})(\vec{a}\cdot\vec{b}) \leqslant |\vec{a}|^2|\vec{b}|^2$, the c_3 term in Eq. (27) will always be larger than the c_1 and c_2 terms.

The three isotropic contributions to the RIXS signal [Eq. (4)] are depicted in the left column of Fig. 4, and the same quantity for the 1D-SXRS signal [Eq. (20)] in the left column of Fig. 5. The first contributions (c_1),

$$S_A(\omega_1,\omega_2) \sim \sum_{e,e'}(\mu_{ge}\cdot\mu_{eg'})(\mu_{ge'}\cdot\mu_{e'g'}), \quad (28)$$

and the second (c_2),

$$S_B(\omega_1,\omega_2) \sim \sum_{e,e'}(\mu_{ge}\cdot\mu_{e'g'})(\mu_{ge'}\cdot\mu_{eg'}), \quad (29)$$

are identical for the RIXS signal but differ in 1D-SXRS. This difference is due to the broad bandwidth in the time-resolved technique, where multiple core-excited states are accessed simultaneously, as opposed to the frequency domain where only one excited state is accessed at a time. In RIXS, therefore, in Eqs. (28) and (29) the sum over e' will only pick out the value for which $e = e'$.

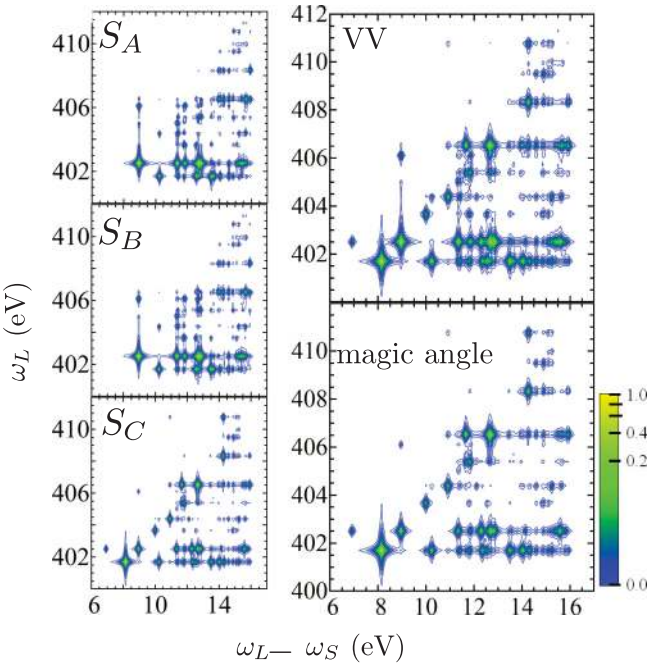

FIG. 4. (Color online) (Left) The three isotropic contributions to the calculated polarized nitrogen K-edge RIXS spectrum of *trans*-NMA. (Right top) RIXS spectra with laser [$E_1(t)$] and detection [$E_2(t)$] fields polarized parallel to each other (both vertically polarized). (Right bottom) Same as top panel but with $E_2(t)$ polarized at the magic angle relative to $E_1(t)$.

In a polarized RIXS experiment the system is excited to an e state by a narrow band polarized laser, and spontaneous emission down to the valence-excited state g' is independently polarized prior to detection. Therefore the f_1 and f_4 tensor components (corresponding to excitation) are parallel to each other, as are f_2 and f_3 (corresponding to emission). The angle between emission and excitation polarizations is θ. Using Eq. (19), we find that the coefficients in Eq. (27) are given by

$$S^{\mathrm{RIXS}}(\omega_1,\omega_2) \propto (3\cos^2\theta - 1, 3\cos^2\theta - 1, 4 - 2\cos^2\theta)\cdot(S_A(\omega_1,\omega_2),\quad S_B(\omega_1,\omega_2),\quad S_C(\omega_1,\omega_2))^T. \quad (30)$$

From Eq. (30) we see that it is possible by choosing a particular value of θ, for which $\cos^2\theta = 1/3$ (referred to as the *magic angle*), to select the $S_C(\omega_1,\omega_2)$ component. The left column of Fig. 4 shows the calculated polarized RIXS signal for the case where the laser and detection are polarized parallel to each other (labeled VV for vertical/vertical) and where the detected light is polarized at the magic angle relative to the laser. As we see in the left panel of Fig. 4, the $S_C(\omega_1,\omega_2)$ contribution is roughly four times larger than the the other two contributions. In the VV signal, the three terms contribute equally so the signal is dominated by the largest. By going to the magic angle it is only possible to remove the $S_A(\omega_1,\omega_2)$ and $S_B(\omega_1,\omega_2)$ contributions, and increase the magnitude of the $S_C(\omega_1,\omega_2)$ contribution. The magic angle signal is consequently about twice the size of the VV signal.

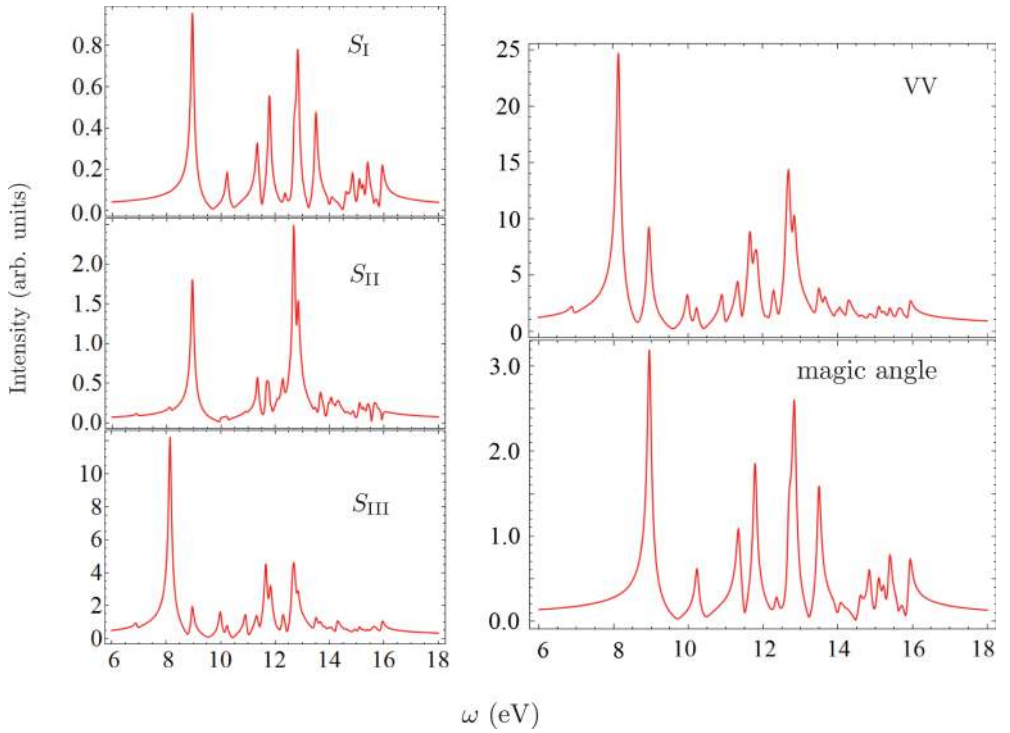

FIG. 5. (Color online) (Left) The three isotropic contributions to the calculated polarized 1D-SXRS spectrum for *trans*-NMA with both pulses tuned to the nitrogen *K* edge. (Right top) 1D-SXRS spectra with both pulses polarized parallel to each other (both vertically polarized). (Right bottom) Same as top panel but with the second pulse (probe) polarized at the magic angle relative to the first pulse (pump).

In a 1D-SXRS experiment, a broadband pulse (the pump) excites the system to a core-excited state then de-excites it to a valence state. The system then evolves for a time τ before the arrival of the probe pulse, which induces another Raman-type transition. After interaction with the probe the system can either be returned to the ground state (left diagram of Fig. 3), or left in a valence-excited state (right diagram of Fig. 3). The signal is defined as the total integrated intensity of the probe pulse with the pump, minus that without the pump (we neglect any stimulated emission or excited-state absorption contributions to this pump probe signal by assuming the delay time τ is long compared with the core-hole lifetime of 7.8 fs). The signal is then Fourier transformed. Only those valence-excited states whose excitation energies are within the pulse bandwidth will contribute to the signal. However, in the time-domain technique one cannot select a particular core-excited state, as all those within the pulse bandwidth will contribute. In this experiment, the f_1 and f_2 vectors are parallel to each other, as are f_3 and f_4. The angle between polarization vectors of the pump and probe is θ. Using Eq. (17), we find that the coefficients in Eq. (27) are given by

$$S_{1D}(\omega_1,\omega_2) \propto (4-2\cos^2\theta, 3\cos^2\theta-1, 3\cos^2\theta-1) \cdot (S_I(\omega_1,\omega_2), \quad S_{II}(\omega_1,\omega_2), \quad S_{III}(\omega_1,\omega_2))^T. \tag{31}$$

The right panel of Fig. 5 shows the calculated VV and magic angle 1D-SXRS signals. The MA thus isolates the $S_I(\omega_1,\omega_2)$ contribution.

It is interesting to note that the largest peak in the VV signal, coming in at 8.14 eV and corresponding to the S_2 CIS state, is missing in the magic angle (MA) signal, where the dominant peak is at 8.95 eV corresponding to the S_3 state. That the S_2 peak does not contribute to the MA signal, can be understood by examination of the spatial distribution of dipoles from this state relative to the dipoles from the ground state. The $S_I(\omega_1,\omega_2)$ contribution to any given peak is proportional to the inner product of μ_{ge} and $\mu_{eg'}$ for all core-excited states within the pulse bandwidth, while the $S_{III}(\omega_1,\omega_2)$ contribution depends only on the magnitude of these dipoles. In the left column of Fig. 6 we show histograms for the angle $\phi \equiv \cos^{-1}(\mu_{ge}\cdot\mu_{eg'}/|\mu_{ge}||\mu_{eg'}|)$ between the upward (from the ground state g to a core excited state e) and downward (from e to a valence excited state g') dipoles for $g' = S_3(\text{top}), S_2(\text{bottom})$. For the majority of core-excited states, the transition dipole to the S_2 state is perpendicular to the dipole to the ground state. For the S_3 state, the distribution of angles between dipoles is more broad and peaked more towards $\phi = 180^\circ$. This explains why the S_3 peak contributes to $S_I(\omega_1,\omega_2)$ (and thus to the magic angle signal), but the S_2 peak does not.

The S_2 peak is the strongest in the $S_{III}(\omega_1,\omega_2)$ component, and thus the strongest peak in the VV signal, due to the large magnitude of the transition dipole between the S_2 state and the first core-excited state. In the right column of Fig. 6 we show calculated absorption spectra from the S_3 and S_2 states. This is the XANES spectrum after preparing the system in a valence-excited state through UV excitation. The amplitude of this signal, shown as sticks under the calculated signals (convoluted with Lorentzian lineshape), is proportional to the squared magnitude of the dipoles to the core-excited states. Absorption from the S_2 state to the first core-excited state is

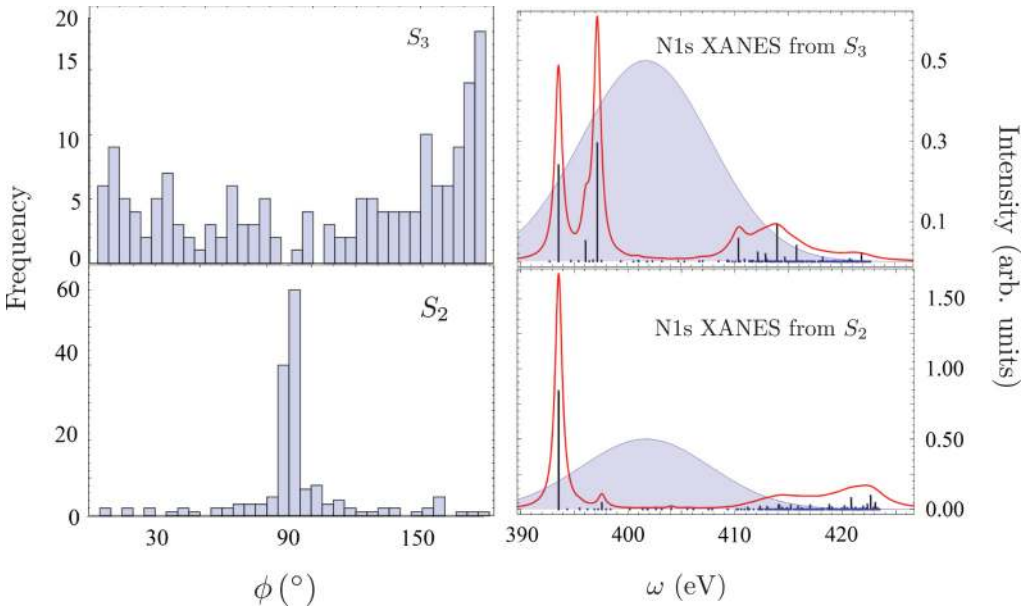

FIG. 6. (Color online) (Left column) Distribution of the angle between μ_{ge} and $\mu_{eg'}$ for all e states with g' equal to S_3 (top) or S_2. The transition dipole from the ground state to a given core-excited state is mostly perpendicular to the dipole from the S_2 state to that same core-excited state. For S_3 this is not the case. (Right column) Calculated XANES spectra assuming that the system is initially in the S_3 state (top) or the S_2 state (bottom).

two to three times larger than absorption from the S_3 state to any of the core-excited state, which is roughly the same as the ratio of the peak amplitudes in the VV 1D-SXRS spectrum in the upper right panel of Fig. 5. This agrees with the fact that the S_2 peak in the VV and magic angle RIXS spectra, coming in at $\omega_L - \omega_S = 8.14\,\text{eV}$, is the strongest peak overall and only has amplitude when the excitation beam is set to the nitrogen core-edge transition at $\omega_L = 401.7\,\text{eV}$.

III. POLARIZATION-DEPENDENT 2D-SXRS

We now extend the polarization-dependent expressions developed for 1D-SXRS to 2D-SXRS. As the 1D signal depends on the dot product of two three-dimensional vectors, one depending on the angle between the pump and probe pulse polarizations, the 2D signal depends on a the dot product of two 15-element vectors, one depending on the three angles between the applied pulses. These three independently varied degrees of freedom do not provide enough control to isolate the isotropic part of the signal in a single experiment. However, we show that a linear combination of two signals can isolate this contribution.

A. The super magic angle pulse configuration

The 2D-SXRS signal is analogous to the 1D signal. The electric field consists of three time-delayed pulses,

$$E^{\text{2D}}(t) = \mathscr{E}_3(t-t_1-t_2)e^{-i\omega_3(t-t_1-t_2)} + \mathscr{E}_2(t-t_1)e^{-i\omega_2(t-t_1)} + \mathscr{E}_1(t)e^{-i\omega_1 t} + \text{c.c.}. \tag{32}$$

The time delays t_1 and t_2 are again taken to be longer than the core-hole lifetime and so any core population created through interaction with the field is ignored in our calculations. The signal is displayed as a frequency-frequency (Ω_1,Ω_2) plot obtained by a Fourier transform of the signal with respect to the delays t_1 and t_2. The diagrams contributing to the signals are shown in Fig. 7. These give

$$S^{2D}(t_1,t_2) = \text{Im}[S_i(t_1,t_2) + S_{ii}(t_1,t_2) + S_{iii}(t_1,t_2) + S_{iv}(t_1,t_2)], \tag{33}$$

where the molecular response function R^{2D} is the sum of four terms (see Fig. 7):

$$\begin{aligned} S_i(t_1,t_2) &= -\langle \alpha_2^\dagger(t_2)\alpha_3(t_2+t_1)\alpha_1(0)\rangle \\ &= -\sum_{g'g''} \alpha_{2;gg''}^{\nu_3\nu_4*}\alpha_{3;g''g'}^{\nu_6\nu_5}\alpha_{1;g'g}^{\nu_2\nu_1} e^{-i(\epsilon_{g'}-i\gamma_{g'})(t_1+t_2)} \\ &\quad \times e^{+i(\epsilon_{g''}+i\gamma_{g''})t_2}, \end{aligned} \tag{34}$$

$$\begin{aligned} S_{ii}(t_1,t_2) &= \langle \alpha_1^\dagger(0)\alpha_2^\dagger(t_1)\alpha_3(t_1+t_2)\rangle \\ &= \sum_{g'g''} \alpha_{1;gg'}^{\nu_1\nu_2*}\alpha_{2;g'g''}^{\nu_3\nu_4*}\alpha_{3;g''g}^{\nu_6\nu_5} e^{+i(\epsilon_{g'}+i\gamma_{g'})t_1} e^{+i(\epsilon_{g''}+i\gamma_{g''})t_2}, \end{aligned} \tag{35}$$

$$\begin{aligned} S_{iii}(t_1,t_2) &= -\langle \alpha_1^\dagger(0)\alpha_3(t_1+t_2)\alpha_2(t_1)\rangle \\ &= -\sum_{g'g''} \alpha_{1;gg'}^{\nu_1\nu_2*}\alpha_{3;g'g''}^{\nu_6\nu_5}\alpha_{2;g''g}^{\nu_4\nu_3} e^{+i(\epsilon_{g'}+i\gamma_{g'})(t_1+t_2)} \\ &\quad \times e^{-i(\epsilon_{g''}-i\gamma_{g''})t_2}, \end{aligned} \tag{36}$$

$$\begin{aligned} S_{iv}(t_1,t_2) &= \langle \alpha_3(t_2+t_1)\alpha_2(t_1)\alpha_1(0)\rangle \\ &= \sum_{g'g''} \alpha_{3;gg''}^{\nu_6\nu_5}\alpha_{2;g''g'}^{\nu_4\nu_3}\alpha_{1;g'g}^{\nu_2\nu_1} e^{-i(\epsilon_{g'}-i\gamma_{g'})t_1} e^{-i(\epsilon_{g''}-i\gamma_{g''})t_2}. \end{aligned} \tag{37}$$

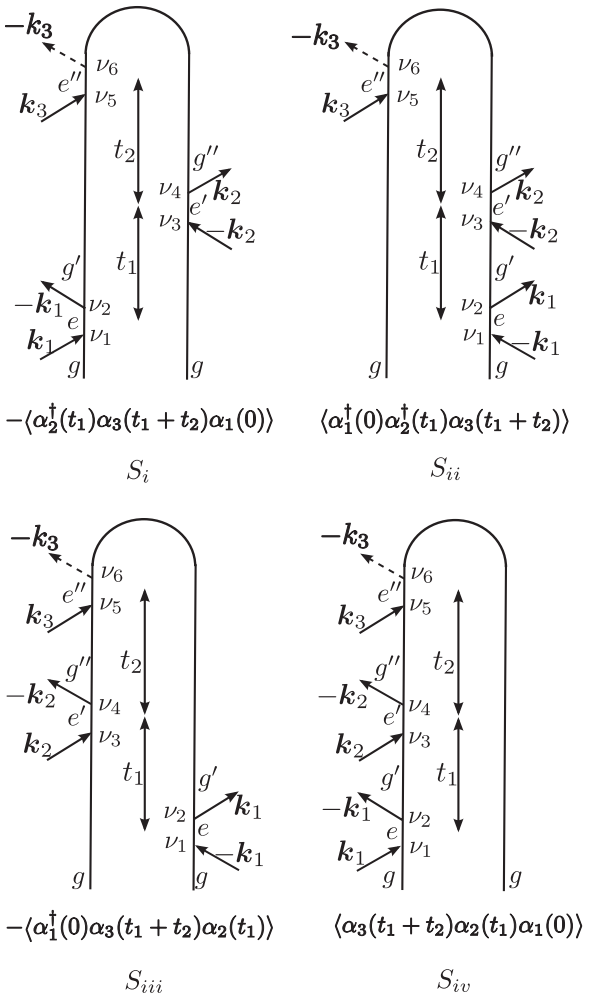

FIG. 7. Diagrams contributing to the 2D-SRS signal.

2D-SXRS is sixth order in the matter-field interaction; rotational averaging is performed using the sixth-order tensor,

$$S^{2D}_{\rm rot}(\theta_{12},\theta_{13},\theta_{23};t_2,t_1)=\sum_{\nu_{1\ldots6}f_{1\ldots6}} S^{2D}_{\nu_1\ldots\nu_6}(t_2,t_1)I^{(6)}_{\nu_1\ldots\nu_6,f_1\ldots f_6} \times e_1^{f_1}e_1^{f_2}e_2^{f_3}e_2^{f_4}e_3^{f_5}e_3^{f_6}, \tag{38}$$

where the analytic form of $I^{(6)}_{\nu_1\ldots\nu_6,f_1\ldots f_6}$ was given in [20], and is reproduced in Appendix A. Performing the contraction in Eq. (38) over the tensor components in Eqs. (38) and (34)–(37), leads to

$$S_{\rm rot}(\theta_{12},\theta_{13},\theta_{23};t_2,t_1)=\mathrm{Im}\,\mathbf{S}_L^T\mathbf{M}\mathbf{V}_R, \tag{39}$$

where

$$\mathbf{S}_L^T=\sum_{\nu_1\ldots\nu_6} S^{2D}_{\nu_1\ldots\nu_6}\mathbf{V}_L^T=(S_{1L},S_{2L},\ldots,S_{15L}) \tag{40}$$

is a vector containing contractions over the different tensor components of Eq. (33). $S_{1L}(t_1,t_2)=S^{2D}_{\rm SMA}(t_1,t_2)$ is the isotropic response,

$$\begin{aligned}S^{2D}_{\rm SMA}(t_1,t_2)=\mathrm{Im}[&-\langle\bar\alpha_2^\dagger(t_2)\bar\alpha_3(t_2+t_1)\bar\alpha_1(0)\rangle\\&+\langle\bar\alpha_1^\dagger(0)\bar\alpha_2^\dagger(t_1)\bar\alpha_3(t_1+t_2)\rangle\\&-\langle\bar\alpha_1^\dagger(0)\bar\alpha_3(t_1+t_2)\bar\alpha_2(t_1)\rangle\\&+\langle\bar\alpha_3(t_2+t_1)\bar\alpha_2(t_1)\bar\alpha_1(0)\rangle].\end{aligned} \tag{41}$$

TABLE I. Angles defining the averaged isotropic signal $S^{\rm SMA}(t_2,t_1)$ in degrees [e.g., $\theta^a_{12}=\arccos(\hat e_{1a}\cdot\hat e_{2a})$; see Fig. 8].

θ^a_{12}	69.3048°
θ^a_{13}	80.1036°
θ^a_{23}	40.5802°
θ^b_{12}	42.6036°
θ^b_{13}	37.0411°
θ^b_{23}	72.5592°

The vector $\mathbf{V}_R\equiv\mathbf{V}_R(\theta_{12},\theta_{13},\theta_{23})$ in Eq. (39) is dependent on the field, a choice of polarizations weights the contributions of the $S_i(t)$ in Eq. (40) to $S^{2D}_{\rm rot}(\theta_{12},\theta_{13},\theta_{23};t_2,t_1)$. The all-parallel signal will be proportional to the equally weighted sum of these vector elements. There are 15 independent pulse configurations. In Appendix B the full expression for $\mathbf{V}_R$ in terms of the angles is given, and we show that no combination of pulse polarizations can isolate $S_{1L}(t_1,t_2)$ in a single measurement, since

$$\mathbf{M}\mathbf{V}_R(\theta_{12},\theta_{13},\theta_{23})\neq\begin{pmatrix}1\\0\\\vdots\\0\end{pmatrix} \tag{42}$$

for all choices of the angles θ_{12}, θ_{13}, and θ_{23}.

The signal is linearly dependent on the vectors $\mathbf{V}_R(\theta_{12},\theta_{13},\theta_{23})$ which are themselves nonlinear functions of the polarization angles. The sum of two signals taken with different pulse polarizations can be written by combining the $\mathbf{V}_R$ vectors. Solving the equation,

$$\mathbf{M}\left[\tfrac{1}{2}\mathbf{V}_{Ra}\left(\theta^a_{12},\theta^a_{13},\theta^a_{23}\right)+\tfrac{1}{2}\mathbf{V}_{Rb}\left(\theta^b_{12},\theta^b_{13},\theta^b_{23}\right)\right]=\begin{pmatrix}1\\0\\\vdots\\0\end{pmatrix} \tag{43}$$

numerically, leads to the angles in Table I. Examples of pulse polarizations with these angles are shown in Fig. 8. One set of pulse polarizations having these angles are given in Fig. 8, and shown in Fig. 13. They define the $S_{\rm SMA}(t_1,t_2)$ technique, which recovers the isotropic signal,

$$\begin{aligned}S^{2D}_{\rm SMA}(t_1,t_2)&=\tfrac{1}{2}S_a(t_1,t_2)+\tfrac{1}{2}S_b(t_1,t_2)\\&=\mathrm{Im}[-\langle\bar\alpha_2^\dagger(t_2)\bar\alpha_3(t_2+t_1)\bar\alpha_1(0)\rangle\\&\quad+\langle\bar\alpha_1^\dagger(0)\bar\alpha_2^\dagger(t_1)\bar\alpha_3(t_1+t_2)\rangle\\&\quad-\langle\bar\alpha_1^\dagger(0)\bar\alpha_3(t_1+t_2)\bar\alpha_2(t_1)\rangle\\&\quad+\langle\bar\alpha_3(t_2+t_1)\bar\alpha_2(t_1)\bar\alpha_1(0)\rangle].\end{aligned} \tag{44}$$

Since these polarizations are not coplanar, the SMA technique requires noncollinear pulses. The 2D-SXRS signal in Eq. (44) recovers the intuitively appealing picture of an applied scalar perturbation driving valence electronic dynamics during the t_1 and t_2 periods.

B. Simulations

The modulus of the nitrogen K-edge 2D-SXRS signals from *trans*-NMA for two different polarization conditions

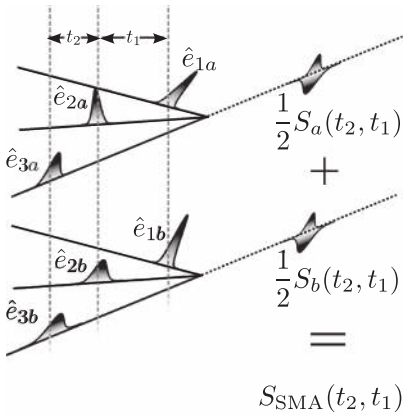

Super Magic Angle pulse polarizations

	x	y	z
$\hat{e}_{1a}$	1.000000	0.000000	0.000000
$\hat{e}_{2a}$	0.353397	−0.609906	−0.709313
$\hat{e}_{3a}$	0.171867	0.000000	−0.985120
$\hat{e}_{1b}$	1.000000	0.000000	0.000000
$\hat{e}_{2b}$	0.736055	−0.479544	−0.477766
$\hat{e}_{3b}$	0.798203	0.000000	0.602388

FIG. 8. (Left) The SMA technique. (Right) The unit vector pulse polarizations ($\hat{e}_{\{1,2,3\}\{a,b\}}$) for each contribution.

are shown in Fig. 9. Peaks in this type of signal come in three different varieties. The diagonal peaks, with $\omega_1 = \omega_2$, are most prominent in the spectrum. This is because the second pulse initiates a Rayleigh-type transition where the coherence created by the first pulse is unchanged by the second, thus accessing the diagonal matrix elements of the effective polarizability for that pulse. Off-diagonal peaks come in two varieties, depending on whether the first and second pulses interact with the same or different (bra/ket) sides of the system density matrix. If the first two pulses interact on the same side, as in diagrams S_{ii} and S_{iv} from Fig. 7, then ω_1 and ω_2 both correspond to valence-excitation frequencies. If the first two pulses interact on different sides, as in diagrams S_i and S_{iii}, then ω_2 will correspond to the *difference* between system excitation frequencies. To emphasize weak features of the signal, we plot the real, imaginary or modulus of the signals using the nonlinear scale $\mathrm{arcsinh}(\zeta) = \ln(\zeta + \sqrt{\zeta^2+1})$ where $\zeta \in \{\mathrm{Re}S, \mathrm{Im}S, |S|^2\}$. This scale is linear for small features and logarithmic for large values. The VVV (all three pulses polarized parallel to each other) and the disentangled SMA signal (denoted as $S_a + S_b$) we show in Fig. 9. Along the top of the spectra, we show a 1D trace along the diagonal of the 2D signals. The SMA signal is the 2D equivalent of

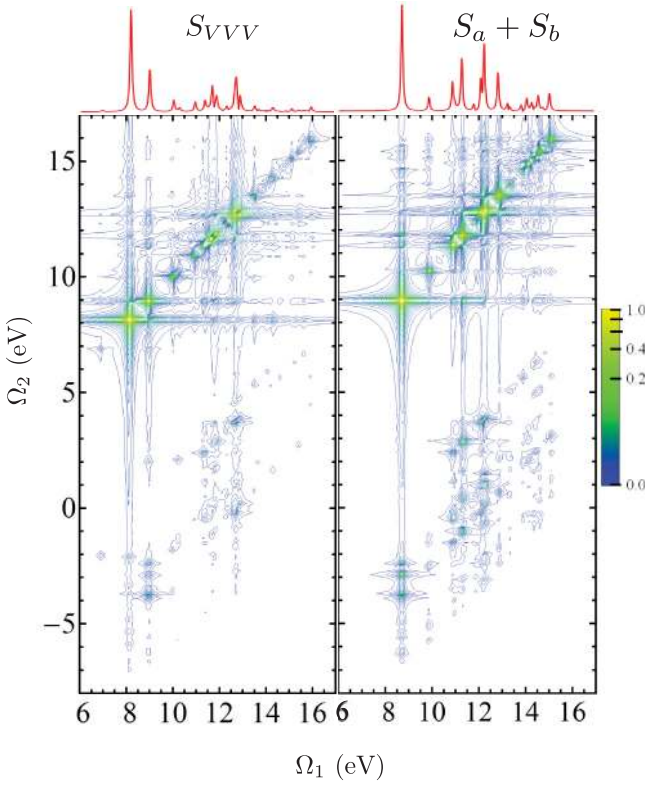

FIG. 9. (Color online) Calculated modulus of the 2D-SXRS signals from *trans*-NMA, using three Gaussian pulses with central frequencies tuned to the nitrogen *K* edge. (Left) Signal taken with all three pulses polarized parallel to each other. The dominant peak is diagonal with $\Omega_1 = \Omega_2 = 8.14$ eV, corresponding the second valence-excited state S_2. (Right) The sum of the S_a and S_b signals defined by Eq. (44). The S_2 peak is completely absent from the SMA signal.

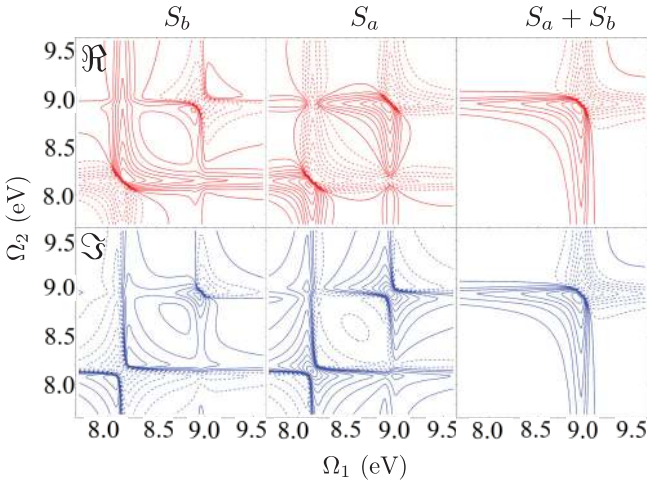

FIG. 10. (Color online) Enlarged portion of the calculated SMA 2D signal described in the text (right), as well as the S_a (left) and S_b (middle) contributions to it. Here we show the real and imaginary parts rather than the modulus, as in Fig. 9, to highlight the interference between the two contributions. The signals are plotted using the same nonlinear scaling as in Fig. 9. The real part of the 2D Fourier transform signals are plotted using red contours, solid for positive values and dashed for negative, and the imaginary parts are plotted with blue contours. The diagonal peak at 8.14 eV is canceled when the S_a and S_b signals are added together, but the 8.95 eV peak is not.

the magic angle in 1D-SXRS in that it isolates the isotropic signal component that depends on the inner product of dipoles that interact with the same pulse. That is, only the contraction $\delta_{\nu_1\nu_2}\delta_{\nu_3\nu_4}\delta_{\nu_5\nu_6}$ will contribute to the disentangled signal, much like only the $\delta_{\nu_1\nu_2}\delta_{\nu_3\nu_4}$ component contributes to the magic angle 1D signal. All 15 isotropic components, listed as $\mathbf{V}_L$ in Eq. (A4), contribute to the VVV signal with equal weight.

The most striking difference between the VVV and SMA signals is that the largest peak in the VVV signal, with $\omega_1 = \omega_2 = 8.14\,\text{eV}$, is absent from the latter. This is analogous to the difference between the VV and magic angle 1D signals, and is again due to the fact that the dipoles from the S_2 state to any core-excited state are perpendicular to the dipoles from that core excited state to the total ground state. In Fig. 10 we show the real and imaginary parts of the S_a and S_b signals, highlighting how the interference between the two leads to a complete cancellation of the S_2 peak.

IV. CONCLUSIONS

We have proposed a specific combination of applied pulse polarizations that allows the 2D Raman signal to be written as correlation functions of the isotropic polarizability simplifying the interpretation of these complex signals. The isotropic vector framework derived in [20] may be used for deriving similar expressions for higher-order stimulated Raman techniques, such as seventh-order Raman spectroscopy. Other terms in the isotropic vector may also prove interesting in examining chiral properties of the material system and the response, as in the four-wave mixing spectroscopy of optical and vibrational systems.

There are many challenges in the theoretical description of polarization-dependent 2D-SXRS in molecules. The isotropic component of the signal is only the most convenient to work with. Other signals with different contractions over the polarizabilities α ($S_{1,2,\ldots}$) may reflect interesting electron-hole dynamics in the valence excited states. Broad principles for identifying parallels between spectral features and electronic dynamics are a continuing area of research, and promise insights in charge and energy transfer in molecules and clusters.

ACKNOWLEDGMENTS

We gratefully acknowledge the support of the Chemical Sciences, Geosciences and Biosciences Division, Office of Basic Energy Sciences, Office of Science, US Department of Energy, the National Science Foundation (Grant No. CHE-1058791), and the National Institutes of Health (Grant No. R01 GM-59230).

APPENDIX A: POLARIZATION-DEPENDENT COMPONENTS OF THE 2D-SRS SIGNAL

The analytic form of $I^{(6)}_{\nu_1\ldots\nu_6,f_1\ldots f_6}$ [20] is

$$I^{\text{rot}}_{\nu_1\ldots\nu_6,f_1\ldots f_6} = \mathbf{V}_L^T\mathbf{M}_6\mathbf{V}_R. \tag{A1}$$

I^{rot} is the product of a vector containing the material tensor components,

$$\mathbf{V}_L = \begin{pmatrix}
\delta_{\nu_1\nu_2}\delta_{\nu_3\nu_4}\delta_{\nu_5\nu_6}\\
\delta_{\nu_1\nu_2}\delta_{\nu_3\nu_5}\delta_{\nu_4\nu_6}\\
\delta_{\nu_1\nu_2}\delta_{\nu_3\nu_6}\delta_{\nu_4\nu_5}\\
\delta_{\nu_1\nu_3}\delta_{\nu_2\nu_4}\delta_{\nu_5\nu_6}\\
\delta_{\nu_1\nu_3}\delta_{\nu_2\nu_5}\delta_{\nu_4\nu_6}\\
\delta_{\nu_1\nu_3}\delta_{\nu_2\nu_6}\delta_{\nu_4\nu_5}\\
\delta_{\nu_1\nu_4}\delta_{\nu_2\nu_3}\delta_{\nu_5\nu_6}\\
\delta_{\nu_1\nu_4}\delta_{\nu_2\nu_5}\delta_{\nu_3\nu_6}\\
\delta_{\nu_1\nu_4}\delta_{\nu_2\nu_6}\delta_{\nu_3\nu_5}\\
\delta_{\nu_1\nu_5}\delta_{\nu_2\nu_3}\delta_{\nu_4\nu_6}\\
\delta_{\nu_1\nu_5}\delta_{\nu_2\nu_4}\delta_{\nu_3\nu_6}\\
\delta_{\nu_1\nu_5}\delta_{\nu_2\nu_6}\delta_{\nu_3\nu_4}\\
\delta_{\nu_1\nu_6}\delta_{\nu_2\nu_3}\delta_{\nu_4\nu_5}\\
\delta_{\nu_1\nu_6}\delta_{\nu_2\nu_4}\delta_{\nu_3\nu_5}\\
\delta_{\nu_1\nu_6}\delta_{\nu_2\nu_5}\delta_{\nu_3\nu_4}
\end{pmatrix}, \tag{A2}$$

a weighting matrix,

$$\mathbf{M}_6 = \frac{1}{210}\begin{pmatrix}
16 & -5 & -5 & -5 & 2 & 2 & -5 & 2 & 2 & 2 & 2 & -5 & 2 & 2 & -5\\
-5 & 16 & -5 & 2 & -5 & 2 & 2 & 2 & -5 & -5 & 2 & 2 & 2 & -5 & 2\\
-5 & -5 & 16 & 2 & 2 & -5 & 2 & -5 & 2 & 2 & -5 & 2 & -5 & 2 & 2\\
-5 & 2 & 2 & 16 & -5 & -5 & -5 & 2 & 2 & 2 & -5 & 2 & 2 & -5 & 2\\
2 & -5 & 2 & -5 & 16 & -5 & 2 & -5 & 2 & -5 & 2 & 2 & 2 & 2 & -5\\
2 & 2 & -5 & -5 & -5 & 16 & 2 & 2 & -5 & 2 & 2 & -5 & -5 & 2 & 2\\
-5 & 2 & 2 & -5 & 2 & 2 & 16 & -5 & -5 & -5 & 2 & 2 & -5 & 2 & 2\\
2 & 2 & -5 & 2 & -5 & 2 & -5 & 16 & -5 & 2 & -5 & 2 & 2 & 2 & -5\\
2 & -5 & 2 & 2 & 2 & -5 & -5 & -5 & 16 & 2 & 2 & -5 & 2 & -5 & 2\\
2 & -5 & 2 & 2 & -5 & 2 & -5 & 2 & 2 & 16 & -5 & -5 & -5 & 2 & 2\\
2 & 2 & -5 & -5 & 2 & 2 & 2 & -5 & 2 & -5 & 16 & -5 & 2 & -5 & 2\\
-5 & 2 & 2 & 2 & 2 & -5 & 2 & 2 & -5 & -5 & -5 & 16 & 2 & 2 & -5\\
2 & 2 & -5 & 2 & 2 & -5 & -5 & 2 & 2 & -5 & 2 & 2 & 16 & -5 & -5\\
2 & -5 & 2 & -5 & 2 & 2 & 2 & 2 & -5 & 2 & -5 & 2 & -5 & 16 & -5\\
-5 & 2 & 2 & 2 & -5 & 2 & 2 & -5 & 2 & 2 & 2 & -5 & -5 & -5 & 16
\end{pmatrix}, \tag{A3}$$

and the field polarization tensor components,

$$\mathbf{V}_R = \begin{pmatrix} \delta_{f_1 f_2}\delta_{f_3 f_4}\delta_{f_5 f_6} \\ \delta_{f_1 f_2}\delta_{f_3 f_5}\delta_{f_4 f_6} \\ \delta_{f_1 f_2}\delta_{f_3 f_6}\delta_{f_4 f_5} \\ \delta_{f_1 f_3}\delta_{f_2 f_4}\delta_{f_5 f_6} \\ \delta_{f_1 f_3}\delta_{f_2 f_5}\delta_{f_4 f_6} \\ \delta_{f_1 f_3}\delta_{f_2 f_6}\delta_{f_4 f_5} \\ \delta_{f_1 f_4}\delta_{f_2 f_3}\delta_{f_5 f_6} \\ \delta_{f_1 f_4}\delta_{f_2 f_5}\delta_{f_3 f_6} \\ \delta_{f_1 f_4}\delta_{f_2 f_6}\delta_{f_3 f_5} \\ \delta_{f_1 f_5}\delta_{f_2 f_3}\delta_{f_4 f_6} \\ \delta_{f_1 f_5}\delta_{f_2 f_4}\delta_{f_3 f_6} \\ \delta_{f_1 f_5}\delta_{f_2 f_6}\delta_{f_3 f_4} \\ \delta_{f_1 f_6}\delta_{f_2 f_3}\delta_{f_4 f_5} \\ \delta_{f_1 f_6}\delta_{f_2 f_4}\delta_{f_3 f_5} \\ \delta_{f_1 f_6}\delta_{f_2 f_5}\delta_{f_3 f_4} \end{pmatrix} = \begin{pmatrix} 1 \\ \cos^2(\theta_{23}) \\ \cos^2(\theta_{23}) \\ \cos^2(\theta_{12}) \\ \cos(\theta_{12})\cos(\theta_{13})\cos(\theta_{23}) \\ \cos(\theta_{12})\cos(\theta_{13})\cos(\theta_{23}) \\ \cos^2(\theta_{12}) \\ \cos(\theta_{12})\cos(\theta_{13})\cos(\theta_{23}) \\ \cos(\theta_{12})\cos(\theta_{13})\cos(\theta_{23}) \\ \cos(\theta_{12})\cos(\theta_{13})\cos(\theta_{23}) \\ \cos(\theta_{12})\cos(\theta_{13})\cos(\theta_{23}) \\ \cos^2(\theta_{13}) \\ \cos(\theta_{12})\cos(\theta_{13})\cos(\theta_{23}) \\ \cos(\theta_{12})\cos(\theta_{13})\cos(\theta_{23}) \\ \cos^2(\theta_{13}), \end{pmatrix}. \tag{A4}$$

θ_{ij} is the angle between polarizations $\hat{e}_i$ and $\hat{e}_j$. Performing the contraction over $\mathbf{V}_L$ in Eq. (A1) and Eqs. (38) and (34)–(37), and relabeling indices such that ν_i refers to the index associated with the ith delta function for each element of $\mathbf{V}_L$, result in the following expressions for the individual signal components S_{1L} through S_{15L}.

$$\begin{aligned} S_{1L}(t_1,t_2) = \sum_{g'g''}\sum_{\nu_1\nu_2\nu_3} & -\alpha^{\nu_2\nu_2*}_{2;gg''}\alpha^{\nu_3\nu_3}_{3;g''g'}\alpha^{\nu_1\nu_1}_{1;g'g}e^{-i(\epsilon_{g'}-i\gamma_{g'})(t_1+t_2)}e^{+i(\epsilon_{g''}+i\gamma_{g''})t_2} + \alpha^{\nu_1\nu_1*}_{1;gg'}\alpha^{\nu_2\nu_2*}_{2;g'g''}\alpha^{\nu_3\nu_3}_{3;g''g}e^{+i(\epsilon_{g'}+i\gamma_{g'})t_1}e^{+i(\epsilon_{g''}+i\gamma_{g''})t_2} \\ & - \alpha^{\nu_1\nu_1*}_{1;gg'}\alpha^{\nu_3\nu_3}_{3;g'g''}\alpha^{\nu_2\nu_2}_{2;g''g}e^{+i(\epsilon_{g'}+i\gamma_{g'})(t_1+t_2)}e^{-i(\epsilon_{g''}-i\gamma_{g''})t_2} + \alpha^{\nu_3\nu_3}_{3;gg''}\alpha^{\nu_2\nu_2}_{2;g''g'}\alpha^{\nu_1\nu_1}_{1;g'g}e^{-i(\epsilon_{g'}-i\gamma_{g'})t_1}e^{-i(\epsilon_{g''}-i\gamma_{g''})t_2}. \end{aligned} \tag{A5}$$

$$\begin{aligned} S_{2L}(t_1,t_2) = \sum_{g'g''}\sum_{\nu_1\nu_2\nu_3} & -\alpha^{\nu_2\nu_3*}_{2;gg''}\alpha^{\nu_3\nu_2}_{3;g''g'}\alpha^{\nu_1\nu_1}_{1;g'g}e^{-i(\epsilon_{g'}-i\gamma_{g'})(t_1+t_2)}e^{+i(\epsilon_{g''}+i\gamma_{g''})t_2} + \alpha^{\nu_1\nu_1*}_{1;gg'}\alpha^{\nu_2\nu_3*}_{2;g'g''}\alpha^{\nu_3\nu_2}_{3;g''g}e^{+i(\epsilon_{g'}+i\gamma_{g'})t_1}e^{+i(\epsilon_{g''}+i\gamma_{g''})t_2} \\ & - \alpha^{\nu_1\nu_1*}_{1;gg'}\alpha^{\nu_3\nu_2}_{3;g'g''}\alpha^{\nu_3\nu_2}_{2;g''g}e^{+i(\epsilon_{g'}+i\gamma_{g'})(t_1+t_2)}e^{-i(\epsilon_{g''}-i\gamma_{g''})t_2} + \alpha^{\nu_3\nu_2}_{3;gg''}\alpha^{\nu_3\nu_2}_{2;g''g'}\alpha^{\nu_1\nu_1}_{1;g'g}e^{-i(\epsilon_{g'}-i\gamma_{g'})t_1}e^{-i(\epsilon_{g''}-i\gamma_{g''})t_2}. \end{aligned} \tag{A6}$$

$$\begin{aligned} S_{3L}(t_1,t_2) = \sum_{g'g''}\sum_{\nu_1\nu_2\nu_3} & -\alpha^{\nu_2\nu_3*}_{2;gg''}\alpha^{\nu_2\nu_3}_{3;g''g'}\alpha^{\nu_1\nu_1}_{1;g'g}e^{-i(\epsilon_{g'}-i\gamma_{g'})(t_1+t_2)}e^{+i(\epsilon_{g''}+i\gamma_{g''})t_2} + \alpha^{\nu_1\nu_1*}_{1;gg'}\alpha^{\nu_2\nu_3*}_{2;g'g''}\alpha^{\nu_2\nu_3}_{3;g''g}e^{+i(\epsilon_{g'}+i\gamma_{g'})t_1}e^{+i(\epsilon_{g''}+i\gamma_{g''})t_2} \\ & - \alpha^{\nu_1\nu_1*}_{1;gg'}\alpha^{\nu_2\nu_3}_{3;g'g''}\alpha^{\nu_3\nu_2}_{2;g''g}e^{+i(\epsilon_{g'}+i\gamma_{g'})(t_1+t_2)}e^{-i(\epsilon_{g''}-i\gamma_{g''})t_2} + \alpha^{\nu_2\nu_3}_{3;gg''}\alpha^{\nu_3\nu_2}_{2;g''g'}\alpha^{\nu_1\nu_1}_{1;g'g}e^{-i(\epsilon_{g'}-i\gamma_{g'})t_1}e^{-i(\epsilon_{g''}-i\gamma_{g''})t_2}. \end{aligned} \tag{A7}$$

$$\begin{aligned} S_{4L}(t_1,t_2) = \sum_{g'g''}\sum_{\nu_1\nu_2\nu_3} & -\alpha^{\nu_1\nu_2*}_{2;gg''}\alpha^{\nu_3\nu_3}_{3;g''g'}\alpha^{\nu_2\nu_1}_{1;g'g}e^{-i(\epsilon_{g'}-i\gamma_{g'})(t_1+t_2)}e^{+i(\epsilon_{g''}+i\gamma_{g''})t_2} + \alpha^{\nu_1\nu_2*}_{1;gg'}\alpha^{\nu_1\nu_2*}_{2;g'g''}\alpha^{\nu_3\nu_3}_{3;g''g}e^{+i(\epsilon_{g'}+i\gamma_{g'})t_1}e^{+i(\epsilon_{g''}+i\gamma_{g''})t_2} \\ & - \alpha^{\nu_1\nu_2*}_{1;gg'}\alpha^{\nu_3\nu_3}_{3;g'g''}\alpha^{\nu_2\nu_1}_{2;g''g}e^{+i(\epsilon_{g'}+i\gamma_{g'})(t_1+t_2)}e^{-i(\epsilon_{g''}-i\gamma_{g''})t_2} + \alpha^{\nu_3\nu_3}_{3;gg''}\alpha^{\nu_2\nu_1}_{2;g''g'}\alpha^{\nu_2\nu_1}_{1;g'g}e^{-i(\epsilon_{g'}-i\gamma_{g'})t_1}e^{-i(\epsilon_{g''}-i\gamma_{g''})t_2}. \end{aligned} \tag{A8}$$

$$\begin{aligned} S_{5L}(t_1,t_2) = \sum_{g'g''}\sum_{\nu_1\nu_2\nu_3} & -\alpha^{\nu_1\nu_3*}_{2;gg''}\alpha^{\nu_3\nu_2}_{3;g''g'}\alpha^{\nu_2\nu_1}_{1;g'g}e^{-i(\epsilon_{g'}-i\gamma_{g'})(t_1+t_2)}e^{+i(\epsilon_{g''}+i\gamma_{g''})t_2} + \alpha^{\nu_1\nu_2*}_{1;gg'}\alpha^{\nu_1\nu_3*}_{2;g'g''}\alpha^{\nu_3\nu_2}_{3;g''g}e^{+i(\epsilon_{g'}+i\gamma_{g'})t_1}e^{+i(\epsilon_{g''}+i\gamma_{g''})t_2} \\ & - \alpha^{\nu_1\nu_2*}_{1;gg'}\alpha^{\nu_3\nu_2}_{3;g'g''}\alpha^{\nu_3\nu_1}_{2;g''g}e^{+i(\epsilon_{g'}+i\gamma_{g'})(t_1+t_2)}e^{-i(\epsilon_{g''}-i\gamma_{g''})t_2} + \alpha^{\nu_3\nu_2}_{3;gg''}\alpha^{\nu_3\nu_1}_{2;g''g'}\alpha^{\nu_2\nu_1}_{1;g'g}e^{-i(\epsilon_{g'}-i\gamma_{g'})t_1}e^{-i(\epsilon_{g''}-i\gamma_{g''})t_2}. \end{aligned} \tag{A9}$$

$$\begin{aligned} S_{6L}(t_1,t_2) = \sum_{g'g''}\sum_{\nu_1\nu_2\nu_3} & -\alpha^{\nu_1\nu_3*}_{2;gg''}\alpha^{\nu_2\nu_3}_{3;g''g'}\alpha^{\nu_2\nu_1}_{1;g'g}e^{-i(\epsilon_{g'}-i\gamma_{g'})(t_1+t_2)}e^{+i(\epsilon_{g''}+i\gamma_{g''})t_2} + \alpha^{\nu_1\nu_2*}_{1;gg'}\alpha^{\nu_1\nu_3*}_{2;g'g''}\alpha^{\nu_2\nu_3}_{3;g''g}e^{+i(\epsilon_{g'}+i\gamma_{g'})t_1}e^{+i(\epsilon_{g''}+i\gamma_{g''})t_2} \\ & - \alpha^{\nu_1\nu_2*}_{1;gg'}\alpha^{\nu_2\nu_3}_{3;g'g''}\alpha^{\nu_3\nu_1}_{2;g''g}e^{+i(\epsilon_{g'}+i\gamma_{g'})(t_1+t_2)}e^{-i(\epsilon_{g''}-i\gamma_{g''})t_2} + \alpha^{\nu_2\nu_3}_{3;gg''}\alpha^{\nu_3\nu_1}_{2;g''g'}\alpha^{\nu_2\nu_1}_{1;g'g}e^{-i(\epsilon_{g'}-i\gamma_{g'})t_1}e^{-i(\epsilon_{g''}-i\gamma_{g''})t_2}. \end{aligned} \tag{A10}$$

$$S_{7L}(t_1,t_2) = \sum_{g'g''}\sum_{\nu_1\nu_2\nu_3} -\alpha^{\nu_2\nu_1*}_{2;gg''}\alpha^{\nu_3\nu_3}_{3;g''g'}\alpha^{\nu_2\nu_1}_{1;g'g}e^{-i(\epsilon_{g'}-i\gamma_{g'})(t_1+t_2)}e^{+i(\epsilon_{g''}+i\gamma_{g''})t_2} + \alpha^{\nu_1\nu_2*}_{1;gg'}\alpha^{\nu_2\nu_1*}_{2;g'g''}\alpha^{\nu_3\nu_3}_{3;g''g}e^{+i(\epsilon_{g'}+i\gamma_{g'})t_1}e^{+i(\epsilon_{g''}+i\gamma_{g''})t_2}$$
$$-\alpha^{\nu_1\nu_2*}_{1;gg'}\alpha^{\nu_3\nu_3}_{3;g'g''}\alpha^{\nu_1\nu_2}_{2;g''g}e^{+i(\epsilon_{g'}+i\gamma_{g'})(t_1+t_2)}e^{-i(\epsilon_{g''}-i\gamma_{g''})t_2} + \alpha^{\nu_3\nu_3}_{3;gg''}\alpha^{\nu_1\nu_2}_{2;g''g'}\alpha^{\nu_2\nu_1}_{1;g'g}e^{-i(\epsilon_{g'}-i\gamma_{g'})t_1}e^{-i(\epsilon_{g''}-i\gamma_{g''})t_2}. \quad \text{(A11)}$$

$$S_{8L}(t_1,t_2) = \sum_{g'g''}\sum_{\nu_1\nu_2\nu_3} -\alpha^{\nu_3\nu_1*}_{2;gg''}\alpha^{\nu_3\nu_2}_{3;g''g'}\alpha^{\nu_2\nu_1}_{1;g'g}e^{-i(\epsilon_{g'}-i\gamma_{g'})(t_1+t_2)}e^{+i(\epsilon_{g''}+i\gamma_{g''})t_2} + \alpha^{\nu_1\nu_2*}_{1;gg'}\alpha^{\nu_3\nu_1*}_{2;g'g''}\alpha^{\nu_3\nu_2}_{3;g''g}e^{+i(\epsilon_{g'}+i\gamma_{g'})t_1}e^{+i(\epsilon_{g''}+i\gamma_{g''})t_2}$$
$$-\alpha^{\nu_1\nu_2*}_{1;gg'}\alpha^{\nu_3\nu_2}_{3;g'g''}\alpha^{\nu_1\nu_3}_{2;g''g}e^{+i(\epsilon_{g'}+i\gamma_{g'})(t_1+t_2)}e^{-i(\epsilon_{g''}-i\gamma_{g''})t_2} + \alpha^{\nu_3\nu_2}_{3;gg''}\alpha^{\nu_1\nu_3}_{2;g''g'}\alpha^{\nu_2\nu_1}_{1;g'g}e^{-i(\epsilon_{g'}-i\gamma_{g'})t_1}e^{-i(\epsilon_{g''}-i\gamma_{g''})t_2}. \quad \text{(A12)}$$

$$S_{9L}(t_1,t_2) = \sum_{g'g''}\sum_{\nu_1\nu_2\nu_3} -\alpha^{\nu_3\nu_1*}_{2;gg''}\alpha^{\nu_2\nu_3}_{3;g''g'}\alpha^{\nu_2\nu_1}_{1;g'g}e^{-i(\epsilon_{g'}-i\gamma_{g'})(t_1+t_2)}e^{+i(\epsilon_{g''}+i\gamma_{g''})t_2} + \alpha^{\nu_1\nu_2*}_{1;gg'}\alpha^{\nu_3\nu_1*}_{2;g'g''}\alpha^{\nu_2\nu_3}_{3;g''g}e^{+i(\epsilon_{g'}+i\gamma_{g'})t_1}e^{+i(\epsilon_{g''}+i\gamma_{g''})t_2}$$
$$-\alpha^{\nu_1\nu_2*}_{1;gg'}\alpha^{\nu_2\nu_3}_{3;g'g''}\alpha^{\nu_1\nu_3}_{2;g''g}e^{+i(\epsilon_{g'}+i\gamma_{g'})(t_1+t_2)}e^{-i(\epsilon_{g''}-i\gamma_{g''})t_2} + \alpha^{\nu_2\nu_3}_{3;gg''}\alpha^{\nu_1\nu_3}_{2;g''g'}\alpha^{\nu_2\nu_1}_{1;g'g}e^{-i(\epsilon_{g'}-i\gamma_{g'})t_1}e^{-i(\epsilon_{g''}-i\gamma_{g''})t_2}. \quad \text{(A13)}$$

$$S_{10L}(t_1,t_2) = \sum_{g'g''}\sum_{\nu_1\nu_2\nu_3} -\alpha^{\nu_2\nu_3*}_{2;gg''}\alpha^{\nu_3\nu_1}_{3;g''g'}\alpha^{\nu_2\nu_1}_{1;g'g}e^{-i(\epsilon_{g'}-i\gamma_{g'})(t_1+t_2)}e^{+i(\epsilon_{g''}+i\gamma_{g''})t_2} + \alpha^{\nu_1\nu_2*}_{1;gg'}\alpha^{\nu_2\nu_3*}_{2;g'g''}\alpha^{\nu_3\nu_1}_{3;g''g}e^{+i(\epsilon_{g'}+i\gamma_{g'})t_1}e^{+i(\epsilon_{g''}+i\gamma_{g''})t_2}$$
$$-\alpha^{\nu_1\nu_2*}_{1;gg'}\alpha^{\nu_3\nu_1}_{3;g'g''}\alpha^{\nu_3\nu_2}_{2;g''g}e^{+i(\epsilon_{g'}+i\gamma_{g'})(t_1+t_2)}e^{-i(\epsilon_{g''}-i\gamma_{g''})t_2} + \alpha^{\nu_3\nu_1}_{3;gg''}\alpha^{\nu_3\nu_2}_{2;g''g'}\alpha^{\nu_2\nu_1}_{1;g'g}e^{-i(\epsilon_{g'}-i\gamma_{g'})t_1}e^{-i(\epsilon_{g''}-i\gamma_{g''})t_2}. \quad \text{(A14)}$$

$$S_{11L}(t_1,t_2) = \sum_{g'g''}\sum_{\nu_1\nu_2\nu_3} -\alpha^{\nu_3\nu_2*}_{2;gg''}\alpha^{\nu_3\nu_1}_{3;g''g'}\alpha^{\nu_2\nu_1}_{1;g'g}e^{-i(\epsilon_{g'}-i\gamma_{g'})(t_1+t_2)}e^{+i(\epsilon_{g''}+i\gamma_{g''})t_2} + \alpha^{\nu_1\nu_2*}_{1;gg'}\alpha^{\nu_3\nu_2*}_{2;g'g''}\alpha^{\nu_3\nu_1}_{3;g''g}e^{+i(\epsilon_{g'}+i\gamma_{g'})t_1}e^{+i(\epsilon_{g''}+i\gamma_{g''})t_2}$$
$$-\alpha^{\nu_1\nu_2*}_{1;gg'}\alpha^{\nu_3\nu_1}_{3;g'g''}\alpha^{\nu_2\nu_3}_{2;g''g}e^{+i(\epsilon_{g'}+i\gamma_{g'})(t_1+t_2)}e^{-i(\epsilon_{g''}-i\gamma_{g''})t_2} + \alpha^{\nu_3\nu_1}_{3;gg''}\alpha^{\nu_2\nu_3}_{2;g''g'}\alpha^{\nu_2\nu_1}_{1;g'g}e^{-i(\epsilon_{g'}-i\gamma_{g'})t_1}e^{-i(\epsilon_{g''}-i\gamma_{g''})t_2}. \quad \text{(A15)}$$

$$S_{12L}(t_1,t_2) = \sum_{g'g''}\sum_{\nu_1\nu_2\nu_3} -\alpha^{\nu_3\nu_3*}_{2;gg''}\alpha^{\nu_2\nu_1}_{3;g''g'}\alpha^{\nu_2\nu_1}_{1;g'g}e^{-i(\epsilon_{g'}-i\gamma_{g'})(t_1+t_2)}e^{+i(\epsilon_{g''}+i\gamma_{g''})t_2} + \alpha^{\nu_1\nu_2*}_{1;gg'}\alpha^{\nu_3\nu_3*}_{2;g'g''}\alpha^{\nu_2\nu_1}_{3;g''g}e^{+i(\epsilon_{g'}+i\gamma_{g'})t_1}e^{+i(\epsilon_{g''}+i\gamma_{g''})t_2}$$
$$-\alpha^{\nu_1\nu_2*}_{1;gg'}\alpha^{\nu_2\nu_1}_{3;g'g''}\alpha^{\nu_3\nu_3}_{2;g''g}e^{+i(\epsilon_{g'}+i\gamma_{g'})(t_1+t_2)}e^{-i(\epsilon_{g''}-i\gamma_{g''})t_2} + \alpha^{\nu_2\nu_1}_{3;gg''}\alpha^{\nu_3\nu_3}_{2;g''g'}\alpha^{\nu_2\nu_1}_{1;g'g}e^{-i(\epsilon_{g'}-i\gamma_{g'})t_1}e^{-i(\epsilon_{g''}-i\gamma_{g''})t_2}. \quad \text{(A16)}$$

$$S_{13L}(t_1,t_2) = \sum_{g'g''}\sum_{\nu_1\nu_2\nu_3} -\alpha^{\nu_2\nu_3*}_{2;gg''}\alpha^{\nu_1\nu_3}_{3;g''g'}\alpha^{\nu_2\nu_1}_{1;g'g}e^{-i(\epsilon_{g'}-i\gamma_{g'})(t_1+t_2)}e^{+i(\epsilon_{g''}+i\gamma_{g''})t_2} + \alpha^{\nu_1\nu_2*}_{1;gg'}\alpha^{\nu_2\nu_3*}_{2;g'g''}\alpha^{\nu_1\nu_3}_{3;g''g}e^{+i(\epsilon_{g'}+i\gamma_{g'})t_1}e^{+i(\epsilon_{g''}+i\gamma_{g''})t_2}$$
$$-\alpha^{\nu_1\nu_2*}_{1;gg'}\alpha^{\nu_1\nu_3}_{3;g'g''}\alpha^{\nu_3\nu_2}_{2;g''g}e^{+i(\epsilon_{g'}+i\gamma_{g'})(t_1+t_2)}e^{-i(\epsilon_{g''}-i\gamma_{g''})t_2} + \alpha^{\nu_1\nu_3}_{3;gg''}\alpha^{\nu_3\nu_2}_{2;g''g'}\alpha^{\nu_2\nu_1}_{1;g'g}e^{-i(\epsilon_{g'}-i\gamma_{g'})t_1}e^{-i(\epsilon_{g''}-i\gamma_{g''})t_2}. \quad \text{(A17)}$$

$$S_{14L}(t_1,t_2) = \sum_{g'g''}\sum_{\nu_1\nu_2\nu_3} -\alpha^{\nu_3\nu_2*}_{2;gg''}\alpha^{\nu_1\nu_3}_{3;g''g'}\alpha^{\nu_2\nu_1}_{1;g'g}e^{-i(\epsilon_{g'}-i\gamma_{g'})(t_1+t_2)}e^{+i(\epsilon_{g''}+i\gamma_{g''})t_2} + \alpha^{\nu_1\nu_2*}_{1;gg'}\alpha^{\nu_3\nu_2*}_{2;g'g''}\alpha^{\nu_1\nu_3}_{3;g''g}e^{+i(\epsilon_{g'}+i\gamma_{g'})t_1}e^{+i(\epsilon_{g''}+i\gamma_{g''})t_2}$$
$$-\alpha^{\nu_1\nu_2*}_{1;gg'}\alpha^{\nu_1\nu_3}_{3;g'g''}\alpha^{\nu_2\nu_3}_{2;g''g}e^{+i(\epsilon_{g'}+i\gamma_{g'})(t_1+t_2)}e^{-i(\epsilon_{g''}-i\gamma_{g''})t_2} + \alpha^{\nu_1\nu_3}_{3;gg''}\alpha^{\nu_2\nu_3}_{2;g''g'}\alpha^{\nu_2\nu_1}_{1;g'g}e^{-i(\epsilon_{g'}-i\gamma_{g'})t_1}e^{-i(\epsilon_{g''}-i\gamma_{g''})t_2}. \quad \text{(A18)}$$

$$S_{15L}(t_1,t_2) = \sum_{g'g''}\sum_{\nu_1\nu_2\nu_3} -\alpha^{\nu_3\nu_3*}_{2;gg''}\alpha^{\nu_1\nu_2}_{3;g''g'}\alpha^{\nu_2\nu_1}_{1;g'g}e^{-i(\epsilon_{g'}-i\gamma_{g'})(t_1+t_2)}e^{+i(\epsilon_{g''}+i\gamma_{g''})t_2} + \alpha^{\nu_1\nu_2*}_{1;gg'}\alpha^{\nu_3\nu_3*}_{2;g'g''}\alpha^{\nu_1\nu_2}_{3;g''g}e^{+i(\epsilon_{g'}+i\gamma_{g'})t_1}e^{+i(\epsilon_{g''}+i\gamma_{g''})t_2}$$
$$-\alpha^{\nu_1\nu_2*}_{1;gg'}\alpha^{\nu_1\nu_2}_{3;g'g''}\alpha^{\nu_3\nu_3}_{2;g''g}e^{+i(\epsilon_{g'}+i\gamma_{g'})(t_1+t_2)}e^{-i(\epsilon_{g''}-i\gamma_{g''})t_2} + \alpha^{\nu_1\nu_2}_{3;gg''}\alpha^{\nu_3\nu_3}_{2;g''g'}\alpha^{\nu_2\nu_1}_{1;g'g}e^{-i(\epsilon_{g'}-i\gamma_{g'})t_1}e^{-i(\epsilon_{g''}-i\gamma_{g''})t_2}. \quad \text{(A19)}$$

APPENDIX B: ISOTROPIC SIGNAL WITH A SINGLE PULSE CONFIGURATION

We attempt to find a combination of pulse polarizations $\{\hat{e}_1,\hat{e}_2,\hat{e}_3\}$ that selects the isotropic part of $\mathbf{V}_L$,

$$\mathbf{M}_6\mathbf{V}_R^{\text{target}} \propto \delta_{\nu_1\nu_2}\delta_{\nu_3\nu_4}\delta_{\nu_5\nu_6}. \quad [=(\mathbf{V}_R)_1] \tag{B1}$$

Following the same approach as the 1D-SRS, we define the target isotropic vector as

$$\left(\mathbf{V}_L^{\text{target}}\right)_1 = (1/27,0,\ldots,0). \tag{B2}$$

The equations the field isotropic polarization vector must obey to isolate this term are

$$\mathbf{V}_R^{\text{target}} = \mathbf{M}_6^{-1}\mathbf{V}_L^{\text{target}} = \begin{pmatrix} 1 \\ 1/3 \\ 1/3 \\ 1/3 \\ 1/9 \\ 1/9 \\ 1/3 \\ 1/9 \\ 1/9 \\ 1/9 \\ 1/9 \\ 1/3 \\ 1/9 \\ 1/9 \\ 1/3 \end{pmatrix} \stackrel{?}{=} \begin{pmatrix} 1 \\ \cos^2(\theta_{23}) \\ \cos^2(\theta_{23}) \\ \cos^2(\theta_{12}) \\ \cos(\theta_{12})\cos(\theta_{13})\cos(\theta_{23}) \\ \cos(\theta_{12})\cos(\theta_{13})\cos(\theta_{23}) \\ \cos^2(\theta_{12}) \\ \cos(\theta_{12})\cos(\theta_{13})\cos(\theta_{23}) \\ \cos(\theta_{12})\cos(\theta_{13})\cos(\theta_{23}) \\ \cos(\theta_{12})\cos(\theta_{13})\cos(\theta_{23}) \\ \cos(\theta_{12})\cos(\theta_{13})\cos(\theta_{23}) \\ \cos^2(\theta_{13}) \\ \cos(\theta_{12})\cos(\theta_{13})\cos(\theta_{23}) \\ \cos(\theta_{12})\cos(\theta_{13})\cos(\theta_{23}) \\ \cos^2(\theta_{13}) \end{pmatrix}. \tag{B3}$$

Equation (B3) reduces to the following set of equations:

$$1/3 = a^2 = b^2 = c^2; \quad 9 = abc, \tag{B4}$$

where

$$a = \cos(\theta_{12}); \quad b = \cos(\theta_{13}); \quad c = \cos(\theta_{23}). \tag{B5}$$

The left part of Eq. (B4) implies that $a,b,c = \pm 1/\sqrt{3}$, which is incompatible with the requirement in the right part that $abc = 1/9$. There is no single combination of pulse polarizations which allow the isotropic response to be extracted. The difference between the 1D-SRS and 2D-SRS cases, is that in the 2D-SRS case the three experimental degrees of freedom for the polarization of the applied pulses, $\{\theta_{12},\theta_{13},\theta_{23}\}$ are not enough to discriminate between the 15 components of the isotropic vectors contributing to the 2D-SRS response. A set of angles chosen to minimize the norm of the difference,

$$\left\|\mathbf{V}_R(\theta_{12},\theta_{13},\theta_{23}) - \mathbf{V}_R^{\text{target}}\right\|, \tag{B6}$$

between any single experiment and the isotropic target vector is given in Fig. 12. The ratio of the first component of this optimized vector to its length,

$$\frac{\mathbf{V}_R\left(\theta_{12}^{\text{opt}},\theta_{13}^{\text{opt}},\theta_{23}^{\text{opt}}\right)_1}{\left|\mathbf{V}_R\left(\theta_{12}^{\text{opt}},\theta_{13}^{\text{opt}},\theta_{23}^{\text{opt}}\right)\right|} = 0.400512, \tag{B7}$$

gives an estimate of how selective a technique is for the isotropic part of the signal. The larger the projection of the $\mathbf{V}_R$ onto the targeted isotropic $\mathbf{V}_R^{\text{target}}$, proportional to its total length, the more strongly the technique selects for the isotropic part of the signal. The result in Eq. (B7) is much better than 1/15 (0.067), which is the all-parallel result and the Dutch cross technique (0.26) which is diagrammed in Fig. 11, and has been used to select against third-order terms in the fifth-order Raman response [27]. This is the best that can be done by a single choice of field polarizations. In the next section the SMA signal is derived, which improves on $\{\theta_{ij}^{\text{opt}}\}$ by taking the linear combination of two signals.

angle	value
θ_{12}^{opt}	57.5859°
θ_{13}^{opt}	122.414°
θ_{23}^{opt}	122.414°

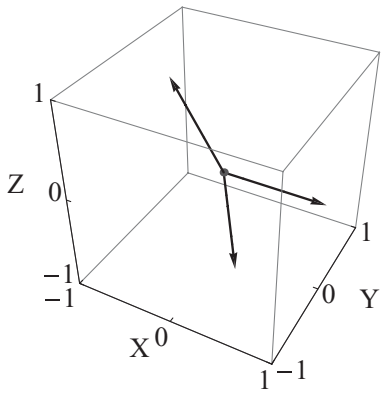

FIG. 11. (Left) Optimum single experiment field polarization angles selective for the isotropic part of the response, and (right) a set of three pulse polarization unit vectors demonstrating these angles.

APPENDIX C: THE SMA TECHNIQUE: ISOTROPIC RESPONSE RECOVERED BY A COMBINATION OF TWO PULSE POLARIZATION CONFIGURATIONS

If the vectors $\mathbf{V}_{L,R}$ were linear functions of $\hat{e}_{1\ldots3}$ the case would be hopeless, but they are not. Consider an experiment with two different pulse configurations $S_a(t_2,t_1)$ and $S_b(t_2,t_1)$. The average signal,

$$S_{\text{SMA}}(t_2,t_1) = \tfrac{1}{2}S_a(t_2,t_1) + \tfrac{1}{2}S_b(t_2,t_1), \tag{C1}$$

is linearly dependent on an effective isotropic field vector,

$$\mathbf{V}_R^{\text{SMA}} = \tfrac{1}{2}\mathbf{V}_R^a + \tfrac{1}{2}\mathbf{V}_R^b, \tag{C2}$$

which is the average of the vectors for each individual experiment. The vectors $\mathbf{V}_R^a$ and $\mathbf{V}_R^b$ are nonlinear functions of the angles $\{\theta_{12}^{a,b},\theta_{13}^{a,b},\theta_{23}^{a,b}\}$. The norm,

$$\left\|\mathbf{V}_R^{\text{SMA}} - \mathbf{V}_R^{\text{target}}\right\|, \tag{C3}$$

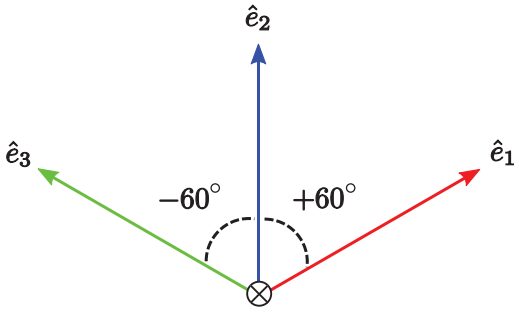

FIG. 12. (Color online) The Dutch cross polarization geometry.

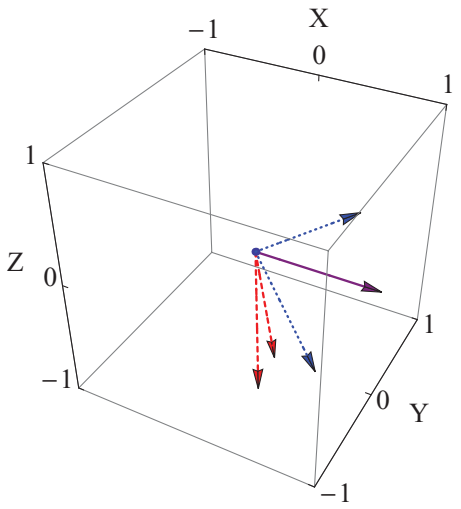

FIG. 13. (Color online) Pulse polarizations contributing to the $S_a(t_2,t_1)$ (red, dashed) and $S_b(t_2,t_1)$ (blue, dotted) signals (The vectors $\hat{e}_{\{1,2,3\}\{a,b\}}$ from Fig. 8). The solid purple vector is the same in both configurations ($\hat{e}_{1a} = \hat{e}_{1b}$).

defined in Eq. (B6) is minimized numerically leading to the angles in Table I, and the pulse polarizations given in Fig. 8 and shown in Fig. 13.

Using this combination of pulse polarizations, the polarizabilities for Eqs. (34)–(37) can be replaced by the isotropic polarizability, and the total signal can be written:

$$S^{2D}_{\mathrm{SMA}}(t_2,t_1) = \tfrac{1}{2}S_a(t_2,t_1) + \tfrac{1}{2}S_b(t_2,t_1) = \mathrm{Re}S_1(t_1,t_2) \quad \text{(C4)}$$

[see Eq. (A5)].

APPENDIX D: FOURIER TRANSFORMED 1D-SXRS

The analytic form of the 1D-SXRS signal is given by writing Eqs. (21)–(23) as sums over terms like

$$f(t) = \mathrm{Re}\left[\sum_{g'} z_A^{g'} e^{-i\epsilon_{g'}\tau-\gamma_{g'}\tau} + z_B^{g'} e^{+i\epsilon_{g'}\tau-\gamma_{g'}\tau}\right]. \quad \text{(D1)}$$

Using the identity

$$\mathrm{Re}(z) = \tfrac{1}{2}(z^* + z), \quad \text{(D2)}$$

the analytic fourier transform of Eq. (D1) is

$$\int_{-\infty}^{\infty} f(t)e^{i\omega t}\mathrm{d}t = \frac{i}{2}\sum_{g'}\frac{\left(z_A^{g'} + z_B^{g'*}\right)}{\omega-\epsilon_{g'}+i\gamma_{g'}} + \frac{\left(z_B^{g'} + z_A^{g'*}\right)}{\omega+\epsilon_{g'}+i\gamma_{g'}}. \quad \text{(D3)}$$

For $S_{I,II,III}(\omega)$, these terms are

$$z_A^{g'} = \alpha_{1;g'g}\alpha_{1;g'g}, \quad \text{(D4)}$$

$$z_B^{g'} = \alpha^*_{1;gg'}\alpha_{2;g'g}, \quad \text{(D5)}$$

with tensor contractions of the operators α that depend on the individual technique. Using this expansion, the Fourier-transformed 1D-SXRS signal is

$$S^{(1D)}_{\mathrm{SXRS}}(\omega) = \tfrac{1}{30}(4-\cos^2\theta)S_{\mathrm{I}}(\omega) + \tfrac{1}{30}(3\cos^2\theta-1)[S_{II}(\omega)+S_{III}(\omega)], \quad \text{(D6)}$$

where

$$S_I(\omega) = \frac{-i}{2}\sum_{g';\nu_1\nu_2}\left[\frac{\alpha^{\nu_1\nu_1}_{1;g'g}\alpha^{\nu_2\nu_2}_{2;gg'} + \alpha^{\nu_1\nu_1}_{1;gg'}\alpha^{\nu_2\nu_2*}_{2;g'g}}{\omega-\epsilon_{g'}+i\gamma_{g'}} + \frac{\alpha^{\nu_1\nu_1*}_{1;gg'}\alpha^{\nu_2\nu_2}_{2;g'g} + \alpha^{\nu_1\nu_1*}_{1;g'g}\alpha^{\nu_2\nu_2*}_{2;gg'}}{\omega+\epsilon_{g'}+i\gamma_{g'}}\right], \quad \text{(D7)}$$

$$S_{II}(\omega) = \frac{-i}{2}\sum_{g';\nu_1\nu_2}\left[\frac{\alpha^{\nu_2\nu_1}_{1;g'g}\alpha^{\nu_2\nu_1}_{2;gg'} + \alpha^{\nu_1\nu_2}_{1;gg'}\alpha^{\nu_1\nu_2*}_{2;g'g}}{\omega-\epsilon_{g'}+i\gamma_{g'}} + \frac{\alpha^{\nu_1\nu_2*}_{1;gg'}\alpha^{\nu_1\nu_2}_{2;g'g} + \alpha^{\nu_2\nu_1*}_{1;g'g}\alpha^{\nu_2\nu_1*}_{2;gg'}}{\omega+\epsilon_{g'}+i\gamma_{g'}}\right], \quad \text{(D8)}$$

$$S_{III}(\omega) = \frac{-i}{2}\sum_{g';\nu_1\nu_2}\left[\frac{\alpha^{\nu_2\nu_1}_{1;g'g}\alpha^{\nu_1\nu_2}_{2;gg'} + \alpha^{\nu_1\nu_2}_{1;gg'}\alpha^{\nu_2\nu_1*}_{2;g'g}}{\omega-\epsilon_{g'}+i\gamma_{g'}} + \frac{\alpha^{\nu_1\nu_2*}_{1;gg'}\alpha^{\nu_2\nu_1}_{2;g'g} + \alpha^{\nu_2\nu_1*}_{1;g'g}\alpha^{\nu_1\nu_2*}_{2;gg'}}{\omega+\epsilon_{g'}+i\gamma_{g'}}\right]. \quad \text{(D9)}$$

APPENDIX E: ROTATIONAL AVERAGING OF 1D-SXRS

For the 1D-SXRS technique, these interactions with the field can be paired into a dynamic polarizability built from the tensor components of the transition dipoles μ_{re} and μ_{es} excited during the Raman interaction with each pulse,

$$\alpha^{\nu_2\nu_1}_{j;rs} \equiv \sum_e \mu^{\nu_2}_{re}\mu^{\nu_1}_{es}\Lambda^{e,j}_{rs}, \quad \text{(E1)}$$

where $\nu_{1,2}$ are polarizations of each dipole, and

$$\Lambda^{e,j}_{rs} = \int_{-\infty}^{\infty}\mathrm{d}\tau_2\int_{-\infty}^{\tau_2}\mathrm{d}\tau_1\mathscr{E}^*_j(\tau_2)\mathscr{E}_j(\tau_1)\exp(i(\omega_j-\omega_{er})\tau_2 - i(\omega_j-\omega_{es})\tau_1) \quad \text{(E2)}$$

is a weighting factor controlled by the central frequencies and widths of the jth pulse. The 1D-SXRS response can be factored into material (ν_j) and field (f_j) tensor products of the transition dipoles and fields, by writing it as correlation functions of this polarizability [see Eq. (11)]:

$$S^{1D}(\omega_1,\omega_2) = \mathrm{Re}[\langle\alpha_2(t_1)\alpha_1(0)\rangle - \langle\alpha^\dagger_1(0)\alpha_2(t_1)\rangle], \quad \text{(E3)}$$

which are dyadic tensors with nine matrix elements,

$$\alpha_{j;rs} = \begin{pmatrix}\alpha^{xx}_{j;rs} & \alpha^{xy}_{j;rs} & \alpha^{xz}_{j;rs}\\ \alpha^{yx}_{j;rs} & \alpha^{yy}_{j;rs} & \alpha^{yz}_{j;rs}\\ \alpha^{zx}_{j;rs} & \alpha^{zy}_{j;rs} & \alpha^{zz}_{j;rs}\end{pmatrix}. \quad \text{(E4)}$$

Expanding the material response in eigenstates, two diagrams contribute (see Fig. 3). The signal,

$$S^{1D}(t) = R^{1D}_{\nu_1\ldots\nu_4}(t)I^{(4)}_{\nu_1\ldots\nu_4,f_1\ldots f_4}(1f_1\hat{e})(1f_2\hat{e})(2f_3\hat{e})(2f_4\hat{e}), \quad \text{(E5)}$$

can be written as the contraction of a material response function R^{1D} tensor with the product of the tensor components of each of the pulse field polarizations ($\hat{e}^i$). In Eq. (E5) and the rest of the document, summation over repeated tensors is assumed.

Each pulse interacts twice with the molecule. Using Eqs. (13) and (14), the molecular response function tensors are

$$R_i^{1D}(t_1) = \frac{i}{\hbar}\langle \alpha_2(t_1)\alpha_1(0)\rangle, \tag{E6}$$

and

$$R_{ii}^{1D}(t) = \frac{i}{\hbar}\langle \alpha_1^{\dagger}(-t_1)\alpha_2(0)\rangle, \tag{E7}$$

corresponding to the diagrams shown in Fig. 3 [9].

[1] J. Marangos, Contemp. Phys. **52**, 551 (2011).
[2] N. Berrah, J. Bozek, J. Costello, S. Düsterer, L. Fang, J. Feldhaus, H. Fukuzawa, M. Hoener, Y. Jiang, P. Johnsson, E. Kennedy, M. Meyer, R. Moshammer, P. Radcliffe, M. Richter, A. Rouzée, A. Rudenko, A. Sorokin, K. Tiedtke, K. Ueda, J. Ullrich, and M. Vrakking, J. Mod. Opt. **57**, 1015 (2010).
[3] J. M. Glownia, J. Cryan, J. Andreasson, A. Belkacem, N. Berrah, C. I. Blaga, C. Bostedt, J. Bozek, L. F. DiMauro, L. Fang, J. Frisch, O. Gessner, M. Ghr, J. Hajdu, M. P. Hertlein, M. Hoener, G. Huang, O. Kornilov, J. P. Marangos, A. M. March, B. K. McFarland, H. Merdji, V. S. Petrovic, C. Raman, D. Ray, D. A. Reis, M. Trigo, J. L. White, W. White, R. Wilcox, L. Young, R. N. Coffee, and P. H. Bucksbaum, Opt. Express **18**, 17620 (2010).
[4] *LCLS: The First Experiments* (Department of Energy, Basic Energy Sciences, Washington, DC, 2000).
[5] S. Shwartz and S. E. Harris, Phys. Rev. Lett. **106**, 080501 (2011).
[6] F. F. Guimarães, V. Kimberg, F. Gel'mukhanov, and H. Ågren, Phys. Rev. A **70**, 062504 (2004).
[7] A. H. Zewail, J. Phys. Chem. A **104**, 5660 (2000).
[8] C. T. Middleton, D. B. Strasfeld, and M. T. Zanni, Opt. Express **17**, 14526 (2009).
[9] S. Mukamel, *Principles of Nonlinear Optical Spectroscopy* (Oxford University Press, Oxford, 1999).
[10] S. Mukamel, Y. Tanimura, and P. Hamm, Acc. Chem. Res. **42**, 1207 (2009).
[11] J. D. Biggs, Y. Zhang, D. Healion, and S. Mukamel, J. Chem. Phys. **136**, 174117 (2012).
[12] B. Patterson, "Resource Letter on Stimulated Inelastic X-ray Scattering at an XFEL," SLAC Technical Note SLAC-TN-10-026 (2010).
[13] Y. Tanimura and S. Mukamel, J. Chem. Phys. **99**, 9496 (1993).
[14] S. Tanaka and S. Mukamel, Phys. Rev. Lett. **89**, 043001 (2002).
[15] I. V. Schweigert and S. Mukamel, Phys. Rev. A **76**, 012504 (2007).
[16] D. Healion, H. Wang, and S. Mukamel, J. Chem. Phys. **134**, 124101 (2011).
[17] V. C. Felicissimo, F. F. Guimaraes, F. Gelmukhanov, A. Cesar, and H. Agren, J. Chem. Phys. **122**, 094319 (2005).
[18] F. F. Guimarães, F. Gel'mukhanov, A. Cesar, and H. Ågren, Chem. Phys. Lett. **405**, 398 (2005).
[19] A. Zholents and G. Penn, Nucl. Instrum. Meth. A **612**, 254 (2010).
[20] D. L. Andrews and T. Thirunamachandran, J. Phys. Chem. **67**, 5026 (1977).
[21] S. Brasselet and J. Zyss, J. Opt. Soc. Am. B **15**, 257 (1998).
[22] B. J. Berne and R. Pecora, *Dynamic Light Scattering: With Applications to Chemistry, Biology, and Physics* (Dover Publications, Mineola, 2000).
[23] K. A. Meyer and J. C. Wright, J. Phys. Chem. A **107**, 8388 (2003).
[24] R. L. Murry, J. T. Fourkas, and T. Keyes, J. Chem. Phys. **109**, 2814 (1998).
[25] R. L. Murry, J. T. Fourkas, and T. Keyes, J. Chem. Phys. **109**, 7913 (1998).
[26] A. Tokmakoff, M. J. Lang, D. S. Larsen, and G. R. Fleming, Chem. Phys. Lett. **272**, 48 (1997).
[27] K. Kubarych, C. Milne, and R. Miller, Chem. Phys. Lett. **369**, 635 (2003).
[28] D. Abramavicius and S. Mukamel, J. Chem. Phys. **122**, 134305 (2005).
[29] J. Cao, J. Wu, and S. Yang, J. Chem. Phys. **116**, 3739 (2002).
[30] J. Wu, J. Cao, and J. T. Fourkas, J. Phys. Chem. A **111**, 9627 (2007).
[31] F. Gel'mukhanov and H. Ågren, Phys. Rep. **312**, 87 (1999).
[32] L. J. P. Ament, M. van Veenendaal, T. P. Devereaux, J. P. Hill, and J. van den Brink, Rev. Mod. Phys. **83**, 705 (2011).
[33] F. De Groot and A. Kotani, *Core Level Spectroscopy of Solids* (CRC Press, Boca Raton, 2008).
[34] F. Gelmukhanov and H. Ågren, Phys. Rev. A **49**, 4378 (1994).
[35] Y. Luo, H. Ågren, and F. Gelmukhanov, Phys. Rev. A **53**, 1340 (1996).
[36] U. Harbola and S. Mukamel, Phys. Rev. B **79**, 085108 (2009).